From silicates to soil carbonates: Tracing the cation budget of microbially-accelerated weathering

AUTHOR NAMES

Corey R. Lawrence[1], Harun Niron[2], Tania Timmermann[1], Philip D. Weyman[1], Yun-Ya Yang[1], Daniel Dores[1], Gonzalo A. Fuenzalida-Meriz[1, *]

AUTHOR ADDRESS

[1] Andes Ag, Inc., Alameda, California, USA

[2] Biobased Sustainability Engineering (SUSTAIN), Department of Bioscience Engineering, University of Antwerp, Antwerp, Belgium

[*] Corresponding Author: Gonzalo A. Fuenzalida-Meriz, gonzalofuenzalida@gmail.com

ABSTRACT

Microbial carbon dioxide mineralization (MCM) is a promising strategy for soil-based carbon dioxide removal (CDR) that leverages beneficial soil microbes applied in agricultural fields to promote native silicate mineral dissolution and carbon drawdown. Unlike enhanced weathering, MCM avoids addition of a mineral feedstock, greatly reducing the carbon footprint from mining, grinding, transporting, and applying the mineral to land. MCM also fits seamlessly into existing farming practices, and the microbial inoculum can be delivered through traditional seed treatments. A key obstacle to measurement, reporting, and verification (MRV) for MCM is ensuring that weathering products are sourced from new silicate dissolution rather than redistribution of pre-existing cations from the exchangeable, oxidizable, or reducible soil pools. To address this, we conducted a 63-day mesocosm study with soybean, applying soil sequential extractions to track

the buildup and distribution of weathering products in soil columns inoculated with *Bacillus subtilis* strain MP1.

Our results indicated that MP1-treated soils yield a net increase in base cations, corresponding to 52.8 mEq column^{-1} relative to the untreated control soils. The majority of base cation increases from silicate weathering were partitioned between the carbonate and exchangeable soil pools, with significant increases of carbonate in the MP1-treated soils. We also observed a significant accumulation of silicon and magnesium in the reducible fraction, suggesting secondary clay mineral formation. However, these changes were small relative to the carbonate and exchangeable fractions. We estimate that 37% to 67% of the dissolution-derived cations formed carbonates, achieving a realized CDR of 0.20 to 0.36 g CO_2 kg^{-1} soil. Overall, our findings support that *Bacillus subtilis* MP1 couples native soil silicate mineral dissolution with carbonate precipitation, confirming MCM as a viable CDR strategy and suggesting soil inorganic carbon measurements as a suitable approach for its MRV.

KEYWORDS

Carbon dioxide removal (CDR), microbial carbon dioxide mineralization (MCM), enhanced weathering (EW), *Bacillus subtilis* strain MP1, soil sequential extraction, soil inorganic carbon (SIC), carbonates, durability.

1. INTRODUCTION

In addition to reducing carbon emissions, technologies enabling carbon dioxide removal (CDR) are needed to reduce the impact of anthropogenic greenhouse gas (GHG) emissions and meet the demands of carbon markets (IPCC, 2022; Smith et al., 2024; Johnstone et al., 2025). Soil-based CDR methods, such as enhanced weathering (EW) and microbial carbon dioxide mineralization (MCM), are appealing because they can be applied in agricultural systems, resulting in co-benefits for soil health and productivity, and where they can be efficiently scaled. The goal of EW is to increase the dissolution of silicate minerals, which is a natural but slow process that acts as a regulator of GHGs over millennial timescales (Walker, Hays & Kasting, 1981; Berner, 1997). There are, however, economic and biogeochemical constraints on this approach that limit its effectiveness in some soil environments. For example, most EW approaches work best in acidic soils, and CDR must be high enough to offset emissions associated with the mining, grinding, transport, and spreading of the feedstock material. Furthermore, the measurement, reporting, and verification (MRV) required for issuance of high-quality carbon credits from soils can be difficult to efficiently apply at scale. In the case of EW, this has led to a variety of different MRV approaches, each with unique costs and benefits (e.g., Clarkson et al., 2024). It is becoming increasingly apparent that there is no 'one size fits all' approach. Technological innovation coupled with applied research will continue to be essential for achieving CDR at the scale required to combat climate change.

Weathering of silicate minerals contained in rocks and soil is a natural negative feedback to increasing atmospheric CO_2, whereby carbonic acid formed from CO_2 and water supplies the acidity needed to drive mineral dissolution. As silicates dissolve, base-cations contained within

71 the minerals are released to solution, and carbon from carbonic acid is converted to carbonate
72 alkalinity (i.e., HCO_3^- + CO_3^{2-}). In natural settings, these reactions are assumed to be too slow to
73 effectively offset anthropogenic GHG emissions. EW approaches increase weathering rates by
74 adding finely crushed mineral feedstocks to soils, accelerating effective weathering rates by
75 increasing the mineral surface area. However, it is becoming increasingly clear that mineral
76 weathering is not strictly an abiotic process; microbes, including bacteria and fungi, have been
77 shown to facilitate and enhance rates of mineral weathering (Finlay et al., 2020; Vicca et al., 2022;
78 Wild et al., 2022; Banfield et al., 1999; Verbruggen et al., 2021; Timmermann et al., 2025; Corbett
79 et al., 2025). There are several hypothesized mechanisms through which microbes may increase
80 mineral weathering, including exudation of carbonic anhydrase enzymes that enhance the
81 solubility of CO_2 and formation of carbonic acid (Xiao et al., 2015; Vicca et al., 2022;
82 Timmermann et al., 2025) or through exudation of organic acids that supply acidity for weathering
83 and act as ligands that remove weathering products (Ribeiro et al., 2020; Vicca et al., 2022; Niron
84 et al., 2025). Harnessing this biological potential may provide another valuable tool to accelerate
85 and scale CDR.
86
87 Microbe-based approaches for accelerating silicate weathering, such as MCM, can be applied to
88 soil systems without the addition of exogenous mineral feedstocks (Timmermann et al., 2025;
89 Gold Standard, 2026). By increasing weathering of preexisting silicate minerals, upfront costs and
90 carbon emissions can be reduced, allowing for more efficient and cost-effective CDR. However,
91 this approach requires soils meeting specific geochemical conditions, and soils must be (1) rich in
92 cation-bearing silicate minerals to be weathered, (2) neutral to alkaline pH (discussed in Yang et
93 al., 2026), and (3) able to precipitate products of mineral dissolution as secondary carbonates.

Timmermann et al. (2025) proposed that accumulation of secondary carbonate minerals, facilitated by microbial amendments, serves as an effective proxy for weathering, allowing for MRV approaches based on carbon rather than base cations. When carbonate formation is coupled with the dissolution of silicates containing divalent cations (Mg^{2+} and Ca^{2+}), which consume two moles of CO_2 for every mole of mineral weathered, half of the CO_2 removed is returned to solution. Carbonate formation therefore reduces the efficiency of CDR from silicate weathering, which is why it is undesirable in traditional EW systems. Yet, without the need for mining, crushing, and transporting feedstock and the associated CO_2 emissions, this process can still allow for cost-effective CDR in a system where only microbial amendments are added to a soil. However, one potential concern with such an approach is that increases in secondary carbonate accumulation could conceivably occur without corresponding increases in silicate weathering, for example, if the divalent cations precipitated in carbonates are sourced from somewhere else in the soil system (e.g., the exchangeable complex). To address this concern and definitively link microbial amendments with increases in silicate dissolution, we conducted an experiment leveraging sequential selective soil extraction, a technique allowing for a comprehensive characterization of the soil weathering system, including tracking of all potential sinks for weathering products (e.g., Steinwidder et al., 2026).

In this study, we describe the results of a laboratory mesocosm experiment, where soybeans were grown with and without the addition of a microbial amendment, *Bacillus subtilis* MP1. We have previously demonstrated that, in both laboratory and field experiments, when soils are amended with strain MP1 or similar microbes, the microbial-acceleration of silicate mineral dissolution can facilitate CDR (Timmermann et al., 2025; Niron et al., 2024). Additionally, we have shown the

potential for these microbial amendments to improve the effectiveness of EW when microbes are added in combination with silicate feedstocks (Yang et al., 2026). However, in both microbial amended and traditional EW systems, questions remain regarding the ultimate fate of weathering products, including base-cations and carbonate alkalinity. To address this uncertainty, we used a sequential selective soil extraction procedure (e.g., Niron et al., 2024; Vienne et al., 2025; Steinwidder et al., 2025) to trace how the microbial amendment MP1 altered silicate weathering and changed various soil base-cation pools. Data from selective sequential extractions provide a powerful way to track products of silicate dissolution and the potential sinks of weathering products. By tracking all inputs and reservoirs of base cations in the experimental system, along with inorganic carbon and other diagnostic soil properties, this work clearly demonstrates that the microbial amendment MP1 facilitates carbonate accumulation by increasing the dissolution of silicate minerals.

2. MATERIALS AND METHODS

2.1. Soil mesocosm experiment. A 63-day soil mesocosm experiment was conducted using 12 soil columns to assess the impact of the microbial amendment *Bacillus subtilis* strain MP1, on soil silicate weathering under soybean (*Glycine max*) cultivation. The soil used for the mesocosm experiment, hereafter referred to as SBX70, was a silty clay soil collected from an agricultural field in Stutsman County, North Dakota, USA. Prior to the mesocosm preparation, the SBX70 soil was sieved through a 10 mm mesh to remove large stones and plant debris, and then manually homogenized. Each mesocosm (35 cm height and 10 cm diameter) was filled with 3 kg of field-moist SBX70 soil to a total height of 30 cm, leaving 5 cm of headspace. After correcting for the moisture content of the soil, this equated to a dry mass of 2.18 kg within each mesocosm.

The experimental design consisted of two treatment groups, each with six biological replicates: (i) untreated control ("UTC") and (ii) MP1 inoculated ("MP1") (Figure S1). MP1 is a naturally occurring *B. subtilis* strain isolated from corn roots and rhizosphere soils. Detailed characterization of MP1 can be found in Timmermann et al. (2025). Each mesocosm was planted with a single soybean seed (Asgrow AG19XF3). To prepare the MP1 treatment, each seed was inoculated with 3.9×10^6 spores of MP1 suspended in 1 mL of distilled water. The concentration of MP1 spores added per mesocosm equates to 3.9×10^3 spores per gram of soil. In the UTC treatment, 1 mL of distilled water per seed was applied instead. The experiment was conducted in a growth chamber under the following conditions: temperature of 22 °C (±5 °C), relative humidity of 65% (±5%), and a 16-hour photoperiod. Plants were watered with deionized (DI) water three times a week for the first six weeks.

2.2. Simulated rainfall events and sample collection. Six weeks (42 days) after sowing and MP1 inoculation, six simulated rainfall events were applied to the mesocosms over a two-week period. The total rainfall amount was 1.75 L of DI water per mesocosm, distributed across the six events, with each mesocosm receiving 292 mL DI water per event. The total volume of water was determined as described in Timmermann et al. (2025). The simulated rainfall schedule followed a pattern of two consecutive days of water additions, followed by two days without, repeating three times, for a total of six simulated rainfall events. Leachate was collected from each mesocosm during each of the six discrete rainfall events, thereby accounting for the total leachate flux throughout the experiment. Following the simulated rainfall period, plants continued to grow under controlled conditions until day 63, at which point they were harvested.

After the 63-day experiment, all 12 mesocosms were harvested and soils were divided into three depth intervals for analyses: 0–10 cm, 10–20 cm, and 20–30 cm (Figure S1). A total of 36 soil samples (two treatments with six replicates and three depths per replicate) were collected and homogenized. Then, the samples were air dried, sieved to 2-mm, and ground for soil physicochemical analyses. Soybean plants were harvested separately for aboveground and belowground biomass.

2.3. Soil chemistry. The total elemental composition of the SBX70 soil prior to the onset of the experiment was measured via x-ray fluorescence (XRF) at the GeoAnalytical Laboratory at Washington State University (Pullman, WA, USA), and soil organic matter content was determined by the loss-on-ignition method at 360 °C (Combs & Nathan, 1998) to allow for normalization of the elemental composition on a volatile-free basis. Technical details and principles underlying these methods are described in Johnson et al. (1999) and Kelly (2018).

Soil inorganic carbon (SIC) was quantified using a gas chromatography (GC) method described in Yip et al. (2025). Soil bicarbonate (HCO_3^-) and carbonate (CO_3^{2-}) ions were quantified using a saturated paste extract followed by titration (Richards L.A., 1954; Yang et al., 2026). Due to the complexity of this measurement, the saturated paste extract was made on a single depth-composited sample from each column. In this study, "carbonate alkalinity" is defined as the combined concentration of HCO_3^- and CO_3^{2-} ions in the soil.

Additional soil physicochemical parameters were analyzed by an external commercial laboratory (Agvise Laboratories, ND, USA). Soil pH was measured using the standard 1:1 soil-to-water ratio method with a calibrated pH meter (Peters et al., 2012). Soil total carbon (TC) was quantified via

dry combustion using a vario MACRO cube elemental analyzer (Elementar Americas Inc., NY), while total soil organic carbon (SOC) was calculated as the difference between TC and SIC (Nelson & Sommers, 1996). Total soil cation exchange capacity was measured using the ammonium acetate displacement method (Sumner & Miller, 1996) and was compared against the sum of exchangeable base cations (described below) to estimate base saturation of the exchange complex, where base saturation (%) is equal to the sum of exchangeable base cations divided by the total cation exchange capacity (both in units of mEq/100g soil).

2.4. Sequential cation extractions. Four soil cation pools were sequentially extracted from soil samples to assess changes in cation mobility and distribution: (1) exchangeable cations, (2) carbonate-bound cations, (3) reducible cations, and (4) the oxidizable fraction. Methodology for sequential extractions was adapted from Tessier et al. (1979) and Uhlig & von Blanckenburg (2019), and is detailed in Steinwidder et al. (2025). In the first step (exchangeable cations), 10 mL of 1 M NH_4OAc was added to 1 g of air-dried soil, shaken for 1 h, centrifuged, and the supernatant collected. For the second step (carbonates), 5 mL of 1 M CH_3COOH was added and shaken for 2 h; then 1 mL of 3 M NH_4OAc was added. Samples were brought to 10 mL with DI water, centrifuged, and supernatants collected. In the third step (reducible — oxide/hydroxide bound cations), 5 mL of 0.05 M NH_2OH in 1 M HCl was added. Samples were heated at 80 °C for 5 h with manual shaking every 30 min, then treated with 3 M NH_4OAc, diluted to 10 mL, centrifuged, and collected. In the final step (oxidizable — organic-bound cations), 4 mL of 30% H_2O_2 in 0.01M HNO_3 was added, and samples were heated at 70 °C with periodic shaking. After 2 h, 3 mL more H_2O_2 was added, and heating continued for 3 h. Then 1 mL of 3 M NH_4OAc was added, samples

were diluted to 10 mL, centrifuged, and collected. Between each step, the soils were rinsed with 10 mL of DI water. All centrifugations were done at 4000 rpm for 10 min, and all extracts were filtered through 0.45 μm filters.

Elemental concentrations were measured using ICP-OES (iCAP 6300 Duo, Thermo Scientific) for Ca, Mg, K, and Na in all cation pools, and for Al, Fe, and Si in the last two pools. Samples were acidified (19:1, 2% HNO_3:sample; TraceMetal Grade, Fisher Chemical) prior to analysis. Calibration used a multi-element standard (CPAChem), with yttrium (Merck) as the internal standard. All standards were diluted in the respective extraction media to ensure matrix-matched calibration and sample conditions.

2.5. Plant biomass & chemistry. At the end of the experiment, above and belowground plant biomass was harvested from each column. Samples were oven dried at 60 °C, then weighed prior to grinding for chemical analyses. Aboveground dry biomass samples were analyzed for elemental composition by ICP-OES following acid digestion at Agvise Laboratories (Northwood ND, USA). Due to lower sample mass from individual columns, an equal mass of belowground biomass from replicate columns were combined, yielding two pooled samples per treatment. The belowground biomass samples were analyzed by ICP-OES following acid digestion at The Pennsylvania State University Agricultural Analytical Service Laboratory (State College PA, USA). To calculate the total cation content attributable to plant above and belowground biomass, measured cation concentrations in plant tissue (mg/kg) were multiplied by plant tissue dry weight.

2.6. Leachate chemistry. Leachate samples, collected from mesocosms following each simulated rainfall event, were analyzed for several biogeochemical parameters. Leachate pH was measured with a benchtop probe following a multipoint calibration. Bicarbonate and CO_3^{2-} ions were quantified via titration with 0.0125 M H_2SO_4 with phenolphthalein and methyl orange indicators (Richards L.A., 1954). Dissolved inorganic carbon (DIC) in leachate was measured on 4 mL of sample following the GC method described in the previous section. Remaining leachate samples were stored frozen and submitted to Agvise Laboratories (Northwood, ND, USA) for analysis of concentrations of soluble cations Ca^{2+}, Mg^{2+}, K^+, and Na^+ (APHA, 1998) as well as major anions including NO_3^-, SO_4^{2-}, and Cl^-. Soil leachate data was assessed for charge balance. Positive charge offsets were assumed to result from sample re-equilibration during the collection phase and were corrected by adjusting total carbonate alkalinity ($HCO_3^- + CO_3^{2-}$) by the corresponding magnitude of the offset (Tosca & Tutolo, 2023).

2.7. Statistical analyses. Based on the distribution and homoscedasticity of the data, either a parametric Student's t-test (normal distribution and equal variance) or a nonparametric Mann–Whitney U test (Wilcoxon rank-sum) was applied to evaluate significant differences ($p < 0.05$) in soil properties among treatments. Statistical analyses of soil and water physicochemical properties were performed using the GraphPad Prism version 10 (GraphPad Software, Boston, Massachusetts, USA) or using tools from the tidyverse packages (Wickham et al., 2019) in R (v4.5.0, R Core Team, 2021).

253 **3. RESULTS**

254 **3.1 Bulk soil and leachate chemistry**

255 **3.1.1. Soil and leachate pH**

256 The initial pH of the SBX70 soil was 7.1 ± 0.03 (N = 3). The volume weighted pH of column
257 leachate was significantly higher ($p < 0.05$, $N = 6$) from the MP1 treatment (8.44 ± 0.04), showing
258 an increase of 0.14 in comparison to the untreated control (8.30 ± 0.06) (Figure 1A). At the end of
259 the experiment, the mean value of soil pH was higher for MP1-treated columns compared with
260 UTC, but the difference was not statistically significant (Figure 1B).

261

262 **3.1.2. Alkalinity and inorganic carbon in soil and leachate**

263 At the end of the 63-day experiment, soil carbonate alkalinity (CO_3^{2-} + HCO_3^-), measured from
264 soil titrations, was significantly higher ($p < 0.05$, $N = 6$) in MP1 compared with UTC columns
265 (Figure 2A). Alkalinity in leachate is reported as the total cumulative flux normalized by the mass
266 of soil in each column (mEq/kg soil) so that it can be directly compared to soil measurements.
267 Leachate alkalinity was similar between treatments, thus, differences between treatments in the
268 total alkalinity of the system (soil + leachate), were mainly driven by the solid phase, resulting in
269 a higher total alkalinity for MP1-treated soils in comparison to UTC soils (Figure 2A). Inorganic
270 carbon in leachate and soil showed similar trends, with higher mean values of SIC and TIC in the
271 MP1 treated columns (≈ 37% increase over UTC) (Figure 2B).

272

273 **3.1.3. Soil total, inorganic and organic carbon**

274 Total soil organic carbon (SOC) from the MP1-treated soil was significantly greater than UTC in
275 the 20-30 cm soil increment ($p < 0.05$, $N = 6$) (Figure 3A). Total inorganic carbon (TIC)

concentrations were near the detection limit of our method for all soils in this study, and though not significant, mean values of MP1-treated soils were consistently higher in TIC across all depth increments (Figure 3B), and at the column level (Figure S2B). When considering the entire column, total carbon was significantly higher ($p < 0.05$, $N = 6$) in the MP1 treatment versus UTC (Figure 3C), and with depth resolution, significant increases in the MP1-treated soils were observed in the 20-30 cm increment (Figure S2A).

3.1.4. Soil cation exchange capacity and column base cation fluxes

Values of total cation exchange capacity ranged from roughly 40 to 47 mEq/100g soil across all treatments and depths, and no clear patterns or significant differences were observed (Figure S3). The total flux of cations in column leachate (calculated as leachate volume collected x concentration) was 5% higher in the MP1 treatment, and all individual base cations were higher in MP1 compared to UTC samples, but differences were not statistically significant (Figure S4).

3.1.5. Plant cation content

Plant biomass was slightly elevated in UTC compared with MP1 columns, but the concentration of base cations tended to be higher in plants from the MP1 column, though neither trend was statistically significant (data not shown). As a result, the overall mass of individual base cations attributable to plant matter was similar for both UTC and MP1 treatments. There were no significant differences observed for the total mass of Mg and K between treatments. The total mass of Ca was higher in MP1 treatment compared with UTC ($p < 0.1$); however, Na was significantly lower in the MP1 treatment compared with UTC ($p < 0.05$, Figure S9).

3.2. Sequential extractions results

3.2.1. Exchangeable fraction

There were no significant differences in exchangeable base cations between treatments, though mean values of exchangeable Ca were consistently higher in MP1-treated columns compared with UTC across all soil depths (Figure S5). Differences in base saturation, calculated as the ratio of the sum of exchangeable base cations to the total cation exchange capacity, were not statistically significant but the mean values were consistently higher for MP1-treated versus UTC columns (Figure S6).

3.2.2. Carbonate fraction

The carbonate extraction yielded some significant differences between MP1 and UTC treatments. In the 10 to 20 cm depth increment, all base cations (Ca, Mg, K, and Na) were significantly higher in the MP1 treatment (Figure 4). Concentrations of K were also significantly greater in the 0-10 and 20-30 cm depth increments.

3.2.3. Reducible fraction

Except for Na in the 10-20 cm depth increment, which was significantly higher in the MP1-treated columns, masses of elements extracted from the reducible pool were comparable between the MP1 and UTC treatments of the top two depth increments (Figure S7). In contrast, masses of Mg and Si extracted from the reducible pool of the 20-30 cm depth increment were significantly greater in the MP1-treated columns compared with UTC (Figure 5). The mean values of all other elements measured (Al, Fe, Ca, K, and Na) were also higher in the MP1-treated columns but differences were not significant at the $p < 0.05$ threshold. The normalized molar ratio of Fe:Mg:Si found in

the reducible fraction of both treatments was on the order of 1:2.5:4 consistent with Si-Mg rich Fe-(hydr)oxides.

3.2.4. Oxidizable fraction

With one exception, there were no significant differences in elemental masses extracted from the oxidizable pool of the MP1 and UTC columns (Figure S8). The exception was Na in the 10 to 20 cm increment, which was near the detection limit for all MP1 columns.

3.3. Cation mass-balance

At the end of the 63-day experiment, the total mass of base cations recovered across all biogeochemical pools measured in this study was higher in the MP1-treated soils compared with UTC soils, for Ca, Mg, and K (Figure 6). In contrast, the total amount of Na recovered was higher in the UTC soils. For Ca and Mg, the two dominant cations in the system, the exchangeable pool represented the largest proportion of the total recovered mass, followed by the carbonate pool (for Ca) and reducible pool (for Mg). Only a small fraction of these cations was associated with the oxidizable, plant biomass, or leachate pools. The pattern for K was consistent with those observed for Mg: most of the recovered K resided in the exchangeable and reducible pools. Whereas the pattern for Na was consistent with those observed for Ca: the two dominant pools were the exchangeable and the carbonate pools. Contrary to the other three cations, the amount of Na recovered from the reducible pool was negligible (Table S3).

4. DISCUSSION

4.1. A conceptual framework for microbe-mediated weathering

Leveraging the soil microbiome to promote carbon dioxide removal represents a promising approach to help offset anthropogenic carbon emissions (Fierer & Walsh, 2023). One such strategy involves using microbes to increase silicate mineral weathering, which converts atmospheric CO_2 to HCO_3^- and carbonates. For example, previous experiments using the plant growth-promoting rhizobacterium *B. subtilis* MP1 (Timmermann et al., 2025; Yang et al., 2026) or other *Bacillus subtilis* strains (Corbett et al., 2025; Niron et al., 2024; Hopf et al., 2009; Song et al., 2007) have suggested promising increases in mineral weathering rates in both laboratory and field environments. This highlights the potential use of microbial amendments as a CDR strategy, and it is hypothesized that increases in mineral weathering driven by these microbes support plant growth through acquisition of rock-derived nutrients (e.g., P, Ca, Mg, K), which are essential for plant growth (Samuels et al., 2020; Dong et al., 2022).

Timmermann et al. (2025) presented a conceptual framework for how these microbes may drive silicate mineral weathering. In this model, microbes facilitate the production of acidity (H^+) via carbonic anhydrases driven catalysis of the conversion of CO_2(aq) to HCO_3^- (e.g., Supuran, 2016) and precipitation of carbonate (which also generates H^+). The protons generated are directed across the microbial biofilm toward the mineral surface where weathering occurs, and the products of weathering are mobilized away from the mineral to facilitate continued dissolution (Figure 4 in Timmermann et al., 2025). This conceptual framework has support in the literature (McConnaughey & Whelan, 1997) but has yet to be fully validated in the context of microbially-mediated weathering. Experimental evidence provides support for the role of secondary carbonate

formation in the context of MP1 amendment (Timmermann et al., 2025). Nonetheless, one concern is that the observed increases in soil carbonate associated with the microbial amendment may source divalent cations from somewhere other than the silicate weathering. To address this question, we conducted a soil mesocosm experiment following the approach described in Timmermann et al. (2025) and Yang et al. (2026), this time incorporating a sequential selective extraction procedure (e.g., Niron et al., 2024; Vienne et al., 2025; Steinwidder et al., 2025; 2026) to trace base cations in available soil reservoirs.

4.2. Bulk soil response to MP1 amendment

Despite being well suited for the MCM approach, with roughly 28% (v/v) feldspars and an initial soil pH of 7.13, the impact of the MP1 microbe amendment was not entirely apparent from bulk soil and leachate data. The flux-weighted pH of the soil leachate was significantly higher from the MP1 columns (Figure 1A), implying a greater consumption of protons, possibly through increased weathering. Soil pH was also elevated in the MP1 treatment compared with control, though differences were not significant (Figure 1B). Similarly, carbonate alkalinity and inorganic carbon content were each higher in the MP1-treated columns (Figure 2), but only soil alkalinity was significant. There were no significant differences in the leachate flux of alkalinity, inorganic carbon, or base cations (Figures 2 and S4). Organic carbon content was significantly higher in the 20-30 cm depth increment (Figure 3A) and, when summed across the entire column, there was significantly greater total carbon in the MP1-treated soils (Figure 3C). Overall, these data provide evidence of increased weathering (higher pH), increased secondary weathering products (soil carbonate alkalinity) and increased soil total carbon associated with MP1 additions, but the magnitude of the response was small relative to natural heterogeneity in other measurements.

These findings are similar to those presented in Yang et al. (2026), and despite patterns suggesting a consistent response to the MP1 amendment, the 63-day experiment may not have been long enough relative to the effect size (Hasemer et al., 2024). By further partitioning the soil into pools or fractions via sequential selective dissolution, we improve our ability to understand these suggestive but inconclusive bulk soil data.

4.3. Cation tracing suggests retention of weathering products in secondary minerals

Selective dissolution is a well-established tool for understanding the distribution of elements across a variety of mineralogic, biologic, or geochemical soil fractions in soils and sediments (Heckman, Lawrence, & Harden, 2018; Wagai & Mayer, 2007; Tessier et al., 1979; and many others). Although there are some potential pitfalls when using such an approach to compare across different soils (e.g., Hass & Fine, 2010; Martin, Nirel, & Thomas, 1987), when applied to a controlled laboratory experiment, partitioning elements between soil 'fractions' or 'pools' provides additional information about sources and sinks associated with changes in the overall system chemistry in response to a treatment. In the context of silicate weathering, this information can be further used to understand the potential implications for CDR (te Pas et al., 2025). The sequential extraction data indicated significant increases in base cations within the carbonate (Figure 4) and reducible (Figure 5) fractions of the MP1-treated columns, with no change in the exchangeable (Figure S5) or oxidizable (Figure S8) fractions.

Given that cation enrichment in carbonate and (hydr)oxides was not accompanied by decreases from any fractions in the MP1-treated columns, remobilization from other depths or fractions is ruled out as a source for the observed increases. Rather, the excess cations, as well as Si and Fe in

414 the reducible fraction, are likely derived from a reservoir not directly quantified with the sequential
415 extraction, with the most likely source being cation-bearing silicate minerals. Increases in Fe and
416 Mg in the reducible fraction are frequently observed following basalt additions (e.g., Niron et al.,
417 2024; Vienne et al., 2025).
418
419 The depth dependence of the observed carbonate (10-20 cm) and reducible fraction base cation
420 enrichments (20-30 cm) within the MP1-treated columns suggest that microbially-enhanced
421 weathering could be spatially variable or that the secondary phases were influenced by the reactive
422 transport and accumulation of weathering products. We did not quantify root abundance with
423 depth, which could have provided insight to the depth distribution of rhizosphere activity.
424 However, because soil respiration generally results in pCO_2 values well above atmospheric levels
425 and the mesocosms are open on the top and bottom, it is reasonable to expect that soil pCO_2 was
426 highest in the intermediate depth. The observed patterns of carbonate and reducible enrichment
427 are consistent with the accumulation of weathering products as porewater infiltrates through the
428 columns. Given that there were no significant differences observed between the treatments in the
429 leachate flux of base cations, it appears that the products of microbially-enhanced weathering were
430 largely retained within the soils.
431
432 The accumulation of weathering-derived base cations in soil pools, sometimes referred to as
433 'cation-scavenging,' influences whether or not the associated CDR is realized (Vienne et al., 2025;
434 Bijma et al., 2026; te Pas et al., 2025; Steinwidder et al., 2025; Hasemer et al., 2024). For the
435 purpose of durable CDR, the ideal scenario is that base cations generated from silicate mineral
436 dissolution are exported from the system in the soil porewater, along with the negatively charged

carbon alkalinity. Due to the constraint of charge balance in solution, when base cations generated from weathering are retained within the soil, the corresponding alkalinity is also retained, and in some cases (e.g., acidic soils) can be converted back to CO_2. However, not all soil sinks for base cations are equivalent (Figure 7). The formation of carbonate minerals results in realized CDR, but only half of what would occur if alkalinity was exported. On the other hand, sequestration of base cations in the exchangeable or oxidizable pools are assumed to delay CDR because those cations can eventually be released and exported (Figure 7). Finally, when base cations accumulate in the reducible pool including secondary hydr(oxides) and clays, or are taken up by plants, CDR is inhibited (te Pas et al., 2025; Vienne et al., 2025; Steinwidder et al., 2025).

The molar ratios of Fe, Mg, and Si in the reducible fraction were generally consistent with formation of Si-Mg rich Fe-(hydr)oxides, which could be a precursor to smectite clays. The eventual formation of smectite would be consistent with normal weathering in these North Dakota soils (Franzen & Bu, 2023). Although both Fe-(hydr)oxides and smectite tend to have high cation exchange capacity (compared with primary silicates), we did not see significant increases in CEC at any depth in the MP1 treatment (Figure S2). However, we did observe a significant increase in organic carbon in the 20-30 cm increment (Figure 3), which could be related to increased (hydr)oxides as suggested by the reducible fraction data. While more work is needed to definitively identify the minerals associated with the reducible fraction and the possible implications for SOC, it is worth noting, compared with EW approaches where exogenous mineral feedstock are applied to the soil, the MCM approach is less likely to generate new forms of secondary minerals that were not already present in the soil.

4.4. The importance of carbonate precipitation in microbially-accelerated weathering

The higher base cation content in the carbonate pool of the MP1-treated columns is consistent with increases in soil carbonate reported in Timmermann et al. (2025) and provides another line of support for the conceptual model presented above, whereby carbonate precipitation is linked to microbially-enhanced silicate weathering. In addition to generating acidity, carbonate formation can serve as a sink for weathering products and could maintain higher rates of weathering by limiting reductions in reaction affinity associated with the accumulation of weathering products (i.e., Maher et al., 2009).

It is noteworthy that the sequential extraction results showed a significant increase in the carbonate fraction from 10-20 cm in MP1 treatment, whereas bulk SIC increases in the MP1 treatment were not significant (Figure S2B). This difference could derive from higher variability of SIC compared with the sequential extraction base cation data, or from SIC values approaching analytical detection limits. The SIC measurements are highly correlated with the total base cations in carbonate extraction (Pearson's r = 0.89, $p < 0.0001$) but estimates of additional carbonate in the MP1 columns from SIC measurements (0.018 mol $CaCO_3$ per column) were higher than the sequential extraction base cation estimates (0.010 mol $CaCO_3$ per column). We attribute this difference to the partial dissolution of newly formed carbonates during the exchangeable cation extraction. Although 1.0 M NH4OAc is widely used to estimate exchangeable cations, it is known to partially dissolve carbonates under some conditions (Tessier et al., 1979; Nel, Bruneel, & Smolders, 2022), potentially leading to an overestimation of exchangeable Ca and Mg and to a corresponding underestimation in the carbonate pool. Furthermore, newly formed biogenic carbonates (e.g., beta calcretes) tend to be fine grained and may be more prone to partial dissolution

(Domínguez-Villar et al., 2022; Wright et al., 1989). Because selective sequential extractions can be susceptible to over- or under-extraction (Hass & Fine, 2010), we assume the SIC-based estimates to be the more accurate measure of the magnitude of soil carbonate.

Based on the mass balance calculations, increases in Ca from the microbial acceleration of silicate weathering was primarily partitioned between the carbonate and exchangeable soil fractions (Figures 6 and 7). However, as discussed above, the sequential extraction method may overestimate the amount of weathering-derived base cations in the exchangeable fraction at the expense of the carbonate fraction. Together these two pools account for the majority of new cations generated through silicate weathering in this soil. The mass of exchangeable Ca (Figure S5) as well as base saturation of the exchange complex (Figure S6) trended higher in the MP1-treated columns but these patterns were not statistically significant, suggesting they may be difficult to detect due to natural soil heterogeneity. Furthermore, in soils with a higher initial base saturation (e.g., Timmermann et al., 2025), we would expect a larger proportion of new Ca to end up in the carbonate fraction. In other words, the base saturation of the soil will influence the efficiency of the carbonate sink, with higher initial degrees of base saturation likely resulting in more carbonate.

There is a large body of evidence demonstrating microbially-mediated carbonate precipitation by an array of different microbes including *Bacillus subtilis* (Zhu & Dittrich, 2016 and reference therein). Moreover, we have previously demonstrated that *B. subtilis* MP1 increases the rate of carbonate precipitation in an alkaline soil (Timmermann et al., 2025). It follows that carbonate precipitation likely occurs in proximity to the MP1 biofilms, and that base cations incorporated within the newly formed carbonates could be removed from solution before they can react with

506 the exchange complex or other cation sinks within the soil. If true, when compared to EW,
507 microbially-mediated weathering may be more resilient to cation scavenging by soil pools that
508 either delay or inhibit CDR (Figure 7).
509
510 **4.5. Cation mass-balance indicates increased silicate weathering in MP1-treated soils**
511 Combining results of the sequential extraction with cation fluxes measured in leachate, and base
512 cations in plant tissue, we found elevated masses of Ca, Mg, and K in the MP1-treated soils,
513 compared to UTC soils (Figure 6). Whereas the total mass of Na decreased in the MP1-treated
514 soils. Taken together, these results provide further support for MP1-driven acceleration of silicate
515 mineral weathering as the ultimate source of the additional cations. On average, the masses of
516 available Ca, Mg, and K in the MP1-treated soils were 6.3%, 2.7%, and 1.1% higher than in the
517 UTC columns, respectively. In contrast, there was a 9.6% reduction of available Na in the MP1-
518 treated columns. However, it should be noted that the magnitudes (Table S3) of MP1-driven
519 changes in Na (-10 mg col^{-1}) and K (+12 mg col^{-1}) were much smaller than Ca (+806 mg col^{-1}) or
520 Mg (+154 mg col^{-1}) and are therefore more likely to be explained by natural heterogeneity or by a
521 limited ability to detect small changes at low concentrations. In total, increases in base cations
522 equate to an average increase of 52.8 mEq of charge per column in the MP1-treated soils, with
523 plant, oxidizable, and leachate fractions accounting for a very small fraction of the total (Figure
524 6). This corresponds to a maximum CDR of 1.1 g CO_2 kg^{-1} soil, assuming all cations from
525 increased silicate weathering are exported from the near field as alkalinity. Based on sequential
526 extraction data, the carbonate fraction accounted for 37% (19.5 mEq col^{-1}) of the overall increase,
527 which is very close to estimates for wollastonite weathering (soil pH = 5.16) reported in te Pas et
528 al. (2025). However, when SIC measurements are used to correct for the potential overextraction

529 of cations in the exchangeable step we estimate the carbonate fraction accounts for as much as
530 35.2 mEq col^{-1} or 67% of new cations from silicate weathering. Carbonate is a less efficient sink
531 for weathering products than export of alkalinity (Figure 7), still the CDR associated with the
532 carbonate fraction accounts for between 0.20 and 0.36 g CO_2 kg^{-1} soil and, importantly, it
533 corresponds to realized CDR.
534
535 **4.6. Considerations of the durability of CDR generated from MCM.**
536 Under field conditions, the fate of the accumulated carbonate will determine durability of the CDR
537 generated through the MCM approach. If the accumulated carbonates are stable in the soil, then
538 the durability of CDR will be at the least equivalent to their residence time in the soil (which can
539 reach millennia, Landi et al., 2003; Monger et al., 2015). On the other hand, if the accumulated
540 carbonates redissolve, then long-term CDR durability will hinge on whether the associated base
541 cations are exported from the system and transported to the ocean (as with traditional EW systems).
542 Raymond, Planavsky, and Reinhard (2025) note that carbonate dissolution in buffered soil systems
543 results in the production of bicarbonate (HCO_3^-) rather than CO_2 outgassing. This is supported by
544 field observations from calcareous agricultural soils demonstrating that, even under active
545 fertilization and nitrification, abiotic CO_2 emissions were negligible (Hodges et al., 2021). Because
546 we have shown that the observed increases in soil carbonate derives from the microbially-mediated
547 acceleration of silicate weathering in a well-buffered soil, subsequent dissolution of the newly
548 formed carbonates would correspond to an additional mole of CDR for every mole of $CaCO_3$
549 dissolved, and the resulting dissolved inorganic carbon will be in the form of HCO_3^- not CO_2. This
550 implies that an MRV approach for MCM based on the accumulation of SIC represents a
551 conservative estimate of the carbon removal, and the resulting CDR is likely to be highly durable.

5. CONCLUSIONS

The results shown in this study further support the application of microbially-accelerated weathering, e.g., MCM, as a viable method of CDR. The sequential selective dissolution measurements and cation mass balance calculations provide strong evidence of silicate weathering increases associated with the MP1 treatment and confirm that secondary carbonate formation plays an important role in this process. Because there was limited evidence of increased base cation or alkalinity export from the experimental mesocosms, the exchangeable and carbonate pools were the primary sinks for weathering derived based cations, with smaller but significant increases also observed in the reducible pool.

By combining the soil sequential selective extraction with measurements of soil leachate and plant biomass, we quantified the overall increase in base cations due to silicate weathering and traced the fate of these weathering products (Figure 7). Our results indicate that between 37 and 67% of weathering driven increases in base cations went to carbonate formation, with the remaining cations retained mainly in the soil exchangeable pool that is assumed to delay CDR. At much smaller magnitudes, the remaining cations were retained in the soil organic pool, representing potential future CDR and in the soil reducible pool and plant fraction, which would constitute no CDR. The range reported for carbonate reflects the possible overextraction of the exchangeable pool, which we constrained with independent measurements of SIC. Our findings suggest caution should be used when comparing sequential extraction results across soils spanning a wide range of pH. In soils with pH greater than ~7, it is also advisable to measure SIC as an independent check on the magnitude of the carbonate fraction.

These results also suggest an advantage of using SIC as the basis for measurement, reporting, and verification (MRV) of CDR in these systems. Although there was a strong correlation between base cation and SIC-based estimates of carbonates, SIC is easier and more cost effective to measure, and in soils with higher pH it may also be more accurate. Furthermore, when MCM is applied in well-buffered soils, an SIC-based MRV approach represents a conservative estimate of CDR. While field-scale studies and modeling should be used to confirm the long-term durability of CDR associated with MCM, the results presented here suggest this approach may have significant benefits compared with traditional EW when applied under appropriate conditions.

ACKNOWLEDGMENTS

The authors thank Dr. Sara Vicca (University of Antwerp) who contributed to early discussions of the selective sequential extraction procedure and provided the laboratory facilities for that work.

REFERENCES

American Public Health Association. (1998). *Standard Methods for the Examination of Water and Wastewater*. Vol. 6. 20th Edition, American Public Health Association (APHA).

Banfield, J. F., Barker, W. W., Welch, S. A., & Taunton, A. (1999). Biological impact on mineral dissolution: application of the lichen model to understanding mineral weathering in the rhizosphere. *Proceedings of the National Academy of Sciences*, 96(7), 3404-3411.

Berner, R. A. (1997). Paleoclimate - The rise of plants and their effect on weathering and atmospheric CO_2. *Science*, 276(5312), 544–546.

Bijma, J., Hagens, M., Hammes, J., Planavsky, N., Pogge von Strandmann, P. A., Reershemius, T., ... & Wolf-Gladrow, D. A. (2025). Reviews and syntheses: Carbon vs. cation based MRV of Enhanced Rock Weathering and the issue of soil organic carbon. *EGUsphere*, 2025, 1-29.

Clarkson, M. O., Larkin, C. S., Swoboda, P., Reershemius, T., Suhrhoff, T. J., Maesano, C. N., & Campbell, J. S. (2024). A review of measurement for quantification of carbon dioxide removal by enhanced weathering in soil. *Frontiers in Climate*, 6, 1345224.

609 Climate Change 2022: Mitigation of Climate Change. Contribution of Working Group III to the
610 Sixth Assessment Report of the Intergovernmental Panel on Climate Change. Cambridge
611 University Press.
612
613 Combs, S. M., and M. V. Nathan. (1998). “Soil Organic Matter.” In *Recommended Chemical Soil*
614 *Test Procedures for the North Central Region*, edited by J. R. Brown, vol. 221, 53–58. Missouri
615 Agriculture Experiment Station.
616
617 Corbett, T., Odelius, E., Uebel, T., Jonsson, T., Singh, A., Vicca, S., Hagens, M., Budnyak, T.,
618 Tkachenko, O., Poetra, R., Hartmann, J., Janssens, I., Niron, H., Van Tendeloo, M., Vlaeminck,
619 S., & Neubeck, A. (2025). Microbial dissolution of Gran Canaria lapilli in small-scale flow through
620 columns: carbon dioxide removal potential. *npj Materials Degradation*, 9(1), 60.
621
622 Domínguez-Villar, D., Bensa, A., Švob, M., & Krklec, K. (2022). Causes and implications of the
623 seasonal dissolution and precipitation of pedogenic carbonates in soils of karst regions–A
624 thermodynamic model approach. *Geoderma*, 423, 115962.
625
626 Gold Standard. (2026). *Microbial carbon di-oxide mineralisation* (Methodology GS4GG PAA
627 M400-04, Version 1.0). Gold Standard for the Global Goals.
628 https://globalgoals.goldstandard.org/standards/458_v1.0_PAA-M400-04_Microbial-Carbon-di-
629 oxide-Mineralisation.pdf
630
631 Dong, H., Huang, L., Zhao, L., Zeng, Q., Liu, X., Sheng, Y., Shi, L., Wu, G., Jiang, H., Li, F.,
632 Zhang, L., Guo, D., Li, G., Hou, W., & Chen, H. (2022). A critical review of mineral–microbe

633 interaction and co-evolution: mechanisms and applications. *National Science Review*, 9(10),
634 nwac128. https://doi.org/10.1093/nsr/nwac128
635
636 Fierer, N., & Walsh, C. M. (2023). Can we manipulate the soil microbiome to promote carbon
637 sequestration in croplands?. *PLoS Biology*, 21(7), e3002207.
638
639 Finlay, R. D., Mahmood, S., Rosenstock, N., Bolou-Bi, E. B., Köhler, S. J., Fahad, Z., ... & Lian,
640 B. (2020). Reviews and syntheses: Biological weathering and its consequences at different spatial
641 levels–from nanoscale to global scale. *Biogeosciences*, 17(6), 1507-1533.
642
643 Hasemer, H., Borevitz, J., & Buss, W. (2024). Measuring enhanced weathering: inorganic carbon-
644 based approaches may be required to complement cation-based approaches. *Frontiers in Climate*,
645 6, 1352825.
646
647 Hass, A., & Fine, P. (2010). Sequential selective extraction procedures for the study of heavy
648 metals in soils, sediments, and waste materials—a critical review. *Critical Reviews in*
649 *Environmental Science and Technology*, 40(5), 365-399.
650
651 Heckman, K., Lawrence, C. R., & Harden, J. W. (2018). A sequential selective dissolution method
652 to quantify storage and stability of organic carbon associated with Al and Fe hydroxide phases.
653 *Geoderma*, 312, 24-35.
654

Hodges, C., Brantley, S. L., Sharifironizi, M., Forsythe, B., Tang, Q., Carpenter, N., & Kaye, J. (2021). Soil carbon dioxide flux partitioning in a calcareous watershed with agricultural impacts. *Journal of Geophysical Research: Biogeosciences*, 126(10), e2021JG006379.

Johnson, D., Hooper, P., & Conrey, R. (1999). XRF method XRF analysis of rocks and minerals for major and trace elements on a single low dilution Li-tetraborate fused bead. *Advances in X-ray Analysis*, *41*, 843-867.

Johnstone, I., Fuss, S., Walsh, N., & Höglund, R. (2025). Carbon markets for carbon dioxide removal. *Climate Policy*, 1–8.

Kelly, D.S. (2018) Analysis of Geological Materials by Low Dilution Fusion at the Peter Hooper GeoAnalytical Lab (Washington State University). Washington State University, Pullman, WA, USA.

Landi, A., Mermut, A. R., & Anderson, D. W. (2003). Origin and rate of pedogenic carbonate accumulation in Saskatchewan soils, Canada. *Geoderma*, 117(1–2), 143–156.

Maher, K., Steefel, C. I., White, A. F., & Stonestrom, D. A. (2009). The role of reaction affinity and secondary minerals in regulating chemical weathering rates at the Santa Cruz Soil Chronosequence, California. *Geochimica et Cosmochimica Acta*, 73(10), 2804-2831.

677 Manning, D. A., & Renforth, P. (2013). Passive sequestration of atmospheric CO2 through coupled
678 plant-mineral reactions in urban soils. *Environmental Science & Technology*, 47(1), 135-141.
679
680 Martin, J. M., Nirel, P., & Thomas, A. J. (1987). Sequential extraction techniques: promises and
681 problems. *Marine Chemistry*, 22(2-4), 313-341.
682
683 McConnaughey, T. A., & Whelan, J. F. (1997). Calcification generates protons for nutrient and
684 bicarbonate uptake. *Earth-Science Reviews*, 42(1–2), 95–117.
685
686 Monger, H. C., Kraimer, R. A., Khresat, S. E., Cole, D. R., Wang, X., & Wang, J. (2015).
687 Sequestration of inorganic carbon in soil and groundwater. *Geology*, 43(5), 375-378.
688
689 Nel, T., Bruneel, Y., & Smolders, E. (2023). Comparison of five methods to determine the cation
690 exchange capacity of soil. *Journal of Plant Nutrition and Soil Science*, 186(3), 311-320.
691
692 Nelson, D. W., and L. E. Sommers. (1996). "Total Carbon, Organic Carbon, and Organic Matter."
693 In *Methods of Soil Analysis: Part 3 Chemical Methods*, edited by D. L. Sparks, A. L.
694
695 Niron, H., Vienne, A., Frings, P., Poetra, R., & Vicca, S. (2024). Exploring the synergy of
696 enhanced weathering and *Bacillus subtilis*: A promising strategy for sustainable agriculture.
697 *Global Change Biology*, 30(9), e17511.
698

699 Niron, H., Calogiuri, T., Singh, A., Neubeck, A., Van Tendeloo, M., Cox, T., ... & Vicca, S. (2025).
700 Alkalinity production and carbon capture from dunite weathering: Individual effects of oxalate,
701 citrate, and EDTA salts. *Chemical Engineering Journal Advances*, 100902.
702
703 Peters, J. B., M. V. Nathan, C. A. M. Laboski, and M. Nathan. 2012. "pH and Lime Requirement.
704 Ch. 4." *In Recommended Chemical Soil Test Procedures for the North Central Region*, vol. 221,
705 16–22. University of Missouri.
706
707 R Core Team (2021). R: A language and environment for statistical computing. *R Foundation for*
708 *Statistical Computing*, Vienna, Austria. URL https://www.R-project.org/.
709
710 Raymond, P., Planavsky, N., & Reinhard, C. T. (2025). Using carbonates for carbon removal.
711 *Nature Water*, 3(8), 844-847.
712
713 Ribeiro, I. D. A., Volpiano, C. G., Vargas, L. K., Granada, C. E., Lisboa, B. B., & Passaglia, L.
714 M. P. (2020). Use of mineral weathering bacteria to enhance nutrient availability in crops: a
715 review. *Frontiers in Plant Science*, 11, 590774.
716
717 Richards, L. A., ed. (1954). *Diagnosis and Improvement of Saline and Alkali Soils (No. 60)*. US
718 Government Printing Office.
719
720 Smith, S. M., Geden, O., Gidden, M. J., Lamb, W. F., Nemet, G. F., Minx, J. C., Buck, H., Burke,
721 J., Cox, E., Edwards, M. R., Fuss, S., Johnstone, I., Müller-Hansen, F., Pongratz, J., Probst, B. S.,

Roe, S., Schenuit, F., Schulte, I., Vaughan, N. E. (eds.) *The State of Carbon Dioxide Removal 2024 - 2nd Edition*. DOI 10.17605/OSF.IO/F85QJ (2024)

Samuels et al. 2020, Microbial weathering of minerals and rocks in natural environments. In: Dontsova K, Balogh-Brunstad Z, Roux GL (eds.). Biogeochemical Cycles: Ecological Drivers and Environmental Impact. Hoboken and Washington, DC: Wiley, 59–79.

Steinwidder, L., Boito, L., Frings, P.J., Niron, H., Rijnders, J., Schutter, A. de, Vienne, A., Vicca, S., (2025). Beyond Inorganic C: Soil Organic C as a Key Pathway for Carbon Sequestration in Enhanced Weathering. *Global Change Biology* 31, e70340.

Steinwidder, L., Boito, L., de Schutter, A., Frings, P. J., Miladinović, N., Niron, H., ... & Vicca, S. (2026). Higher Inorganic CO2 Removal Despite Slower Weathering in an Enhanced Weathering Experiment With Steel Slags and Basalt. *Global Change Biology*, 32(1), e70666.

Sumner, M. E., and W. P. Miller. 1996. "Cation Exchange Capacity and Exchange Coefficients." In *Methods of Soil Analysis: Part 3 Chemical Methods*, edited by D. L. Sparks, A. L. Page, P. A. Helmke, et al., vol. 5, 1201–1229. American Society of Agronomy, Crop Science Society of America, and Soil Science Society of America.

Supuran, C. T. (2016). Structure and function of carbonic anhydrases. *Biochemical Journal*, 473(14), 2023-2032.

te Pas, E. E. E. M. te, Chang, E., Marklein, A. R., Comans, R. N. J., & Hagens, M. (2025). Accounting for retarded weathering products in comparing methods for quantifying carbon dioxide removal in a short-term enhanced weathering study. *Frontiers in Climate*, 6, 1524998.

Timmermann, T., Yip, C., Yang, Y., Wemmer, K.A., Chowdhury, A., Dores, D., Takayama, T., Nademanee, S., Traag, B.A., Zamanian, K., González, B., Breecker, D.O., Fierer, N., Slessarev, E.W., Fuenzalida-Meriz, G.A. (2025). Harnessing Microbes to Weather Native Silicates in Agricultural Soils for Scalable Carbon Dioxide Removal. *Global Change Biology* 31(5), e70216.

Tessier, A. P. G. C., Campbell, P. G., & Bisson, M. J. A. C. (1979). Sequential extraction procedure for the speciation of particulate trace metals. *Analytical Chemistry*, 51(7), 844-851.

Tosca, N.J. & Tutolo, B.M., (2023). Alkalinity in Theory and Practice. *Elements* 19, 7–9.

Uhlig, D., & Von Blanckenburg, F. (2019). How slow rock weathering balances nutrient loss during fast forest floor turnover in montane, temperate forest ecosystems. *Frontiers in Earth Science*, 7, 159.

Uroz, S., Calvaruso, C., Turpault, M. P., & Frey-Klett, P. (2009). Mineral weathering by bacteria: ecology, actors and mechanisms. *Trends in Microbiology*, 17(8), 378-387.

Verbruggen, E., Struyf, E., & Vicca, S. (2021). Can arbuscular mycorrhizal fungi speed up carbon sequestration by enhanced weathering?. *Plants, People, Planet*, 3(5), 445-453.

Vicca, S., Goll, D. S., Hagens, M., Hartmann, J., Janssens, I. A., Neubeck, A., ... & Verbruggen, E. (2022). Is the climate change mitigation effect of enhanced silicate weathering governed by biological processes?. *Global Change Biology*, 28(3), 711-726.

Vienne, A., Frings, P., Rijnders, J., Suhrhoff, T.J., Reershemius, T., Poetra, R.P., Hartmann, J., Niron, H., Estrada, M.P., Steinwidder, L., Boito, L., Vicca, S., (2025). Weathering without inorganic CDR revealed through cation tracing. *EGUsphere* 2025, 1–24. doi:10.5194/egusphere-2025-1667

Wagai, R., & Mayer, L. M. (2007). Sorptive stabilization of organic matter in soils by hydrous iron oxides. *Geochimica et Cosmochimica Acta*, 71(1), 25-35.

Walker, J. C. G., Hays, P. B., & Kasting, J. F. (1981). A negative feedback mechanism for the long-term stabilization of Earth's surface temperature. *Journal of Geophysical Research*, 86(C10): 9776–9782.

Wild, B., Gerrits, R., & Bonneville, S. (2022). The contribution of living organisms to rock weathering in the critical zone. *npj Materials degradation*, 6(1), 98.

Wickham H, Averick M, Bryan J, Chang W, McGowan LD, François R, Grolemund G, Hayes A, Henry L, Hester J, Kuhn M, Pedersen TL, Miller E, Bache SM, Müller K, Ooms J, Robinson D,

790 Seidel DP, Spinu V, Takahashi K, Vaughan D, Wilke C, Woo K, Yutani H (2019). Welcome to
791 the tidyverse. *Journal of Open Source Software*, 4(43), 1686. doi:10.21105/joss.01686.
792
793 Wright, V. P. (1989). Terrestrial stromatolites and laminar calcretes: a review. *Sedimentary*
794 *Geology*, 65(1-2), 1-13.
795
796 Xiao, L., Lian, B., Hao, J., Liu, C., & Wang, S. (2015). Effect of carbonic anhydrase on silicate
797 weathering and carbonate formation at present day CO2 concentrations compared to primordial
798 values. *Scientific Reports*, 5(1), 7733.
799
800 Yang, Y. Y., de Mesquita, C. P. B., Lawrence, C. R., Weyman, P. D., Dores, D., Timmermann,
801 T., Fierer, N., & Fuenzalida-Meriz, G. A. (2026). Synergistic Effects of a Microbial Amendment
802 and Crushed Basalt: Soil Geochemical and Microbial Responses. *Global Change Biology* 32(1),
803 e70705.
804
805 Yip, C., Weyman, P. D., Wemmer, K. A., Yang, Y. Y., Chowdhury, A., Traag, B. A.,
806 Timmermann, T., & Fuenzalida-Meriz, G. (2025). Quantification of soil inorganic carbon using
807 sulfamic acid and gas chromatography. *PLoS One*, 20(5), e0320778.
808
809 Zhu T and Dittrich M (2016) Carbonate Precipitation through Microbial Activities in Natural
810 Environment, and Their Potential in Biotechnology: A Review. *Frontiers in Bioengineering and*
811 *Biotechnology.* 4:4. doi: 10.3389/fbioe.2016.0000
812

FIGURES

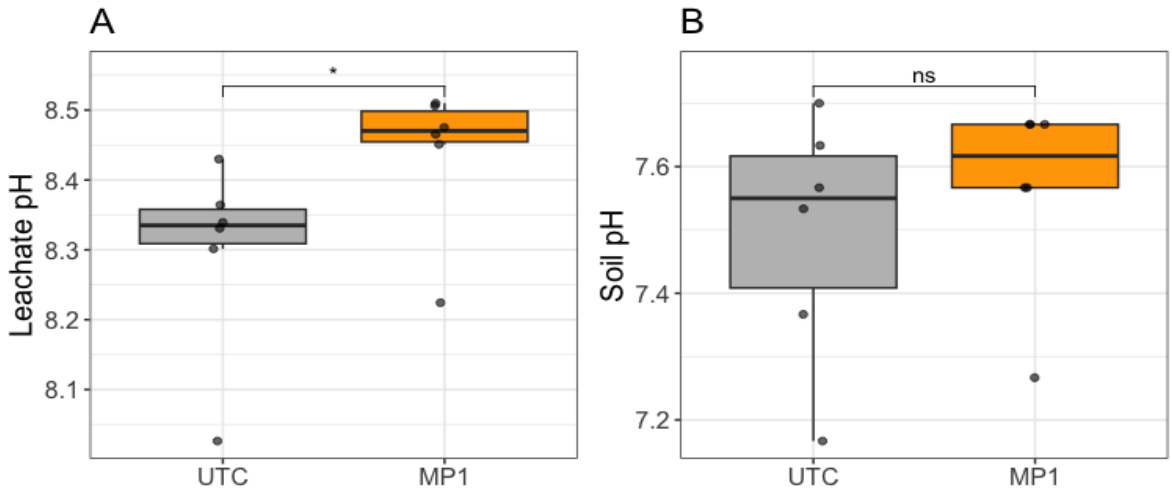

Figure 1. Leachate pH **(A)** and soil pH **(B)** in MP1-treated and untreated control (UTC) columns. Wilcoxon signed-rank test, * $p < 0.05$, ns: not significant, $N = 6$. Note that y-axes are scaled to the data range to clearly visualize the distribution and variability across treatments.

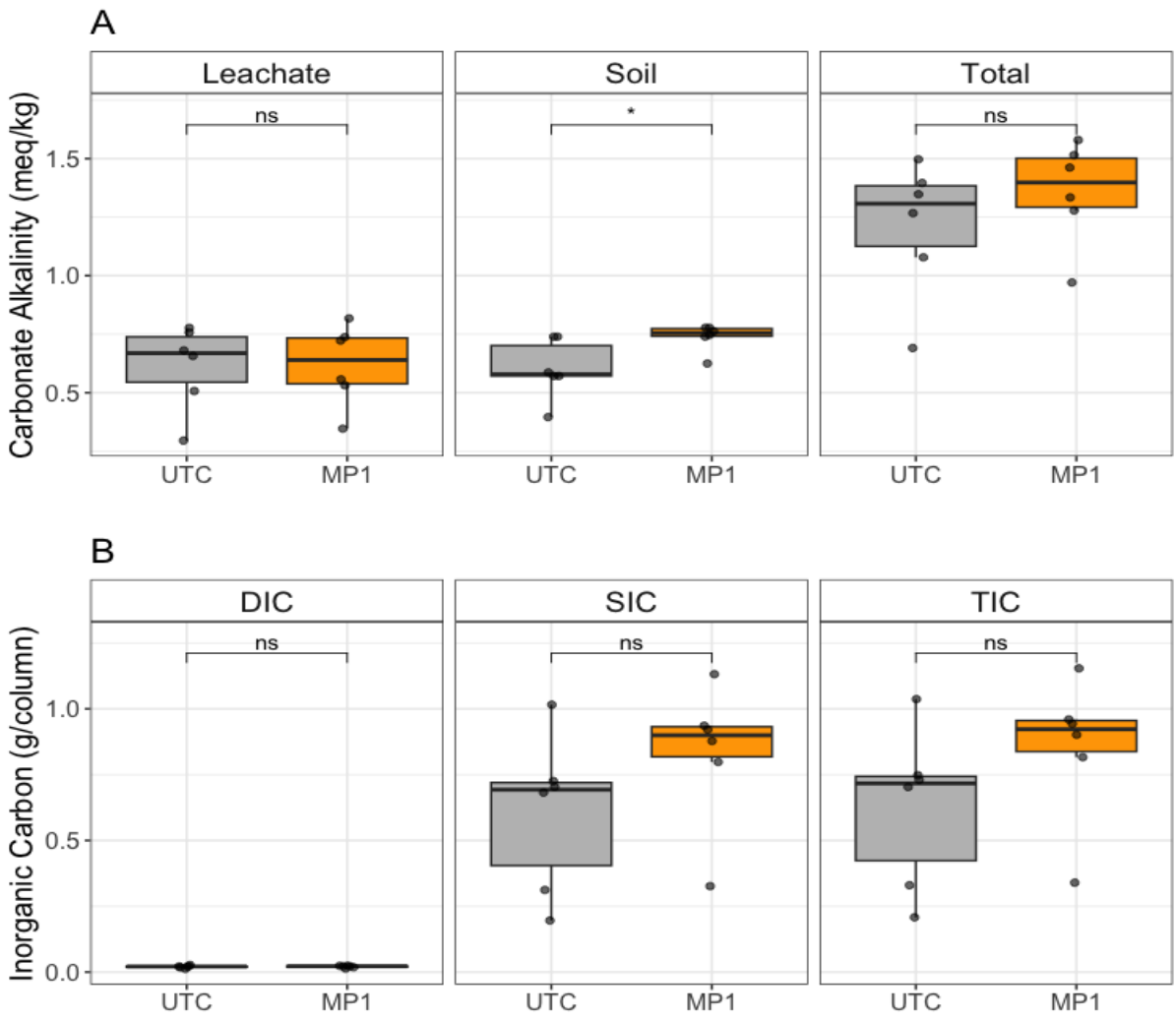

819

820 **Figure 2.** Carbonate alkalinity **(A)** and inorganic carbon **(B)** in MP1-treated and untreated control

821 (UTC) columns. Student's t-test, * $p < 0.05$, ns: not significant, $N = 6$.

822

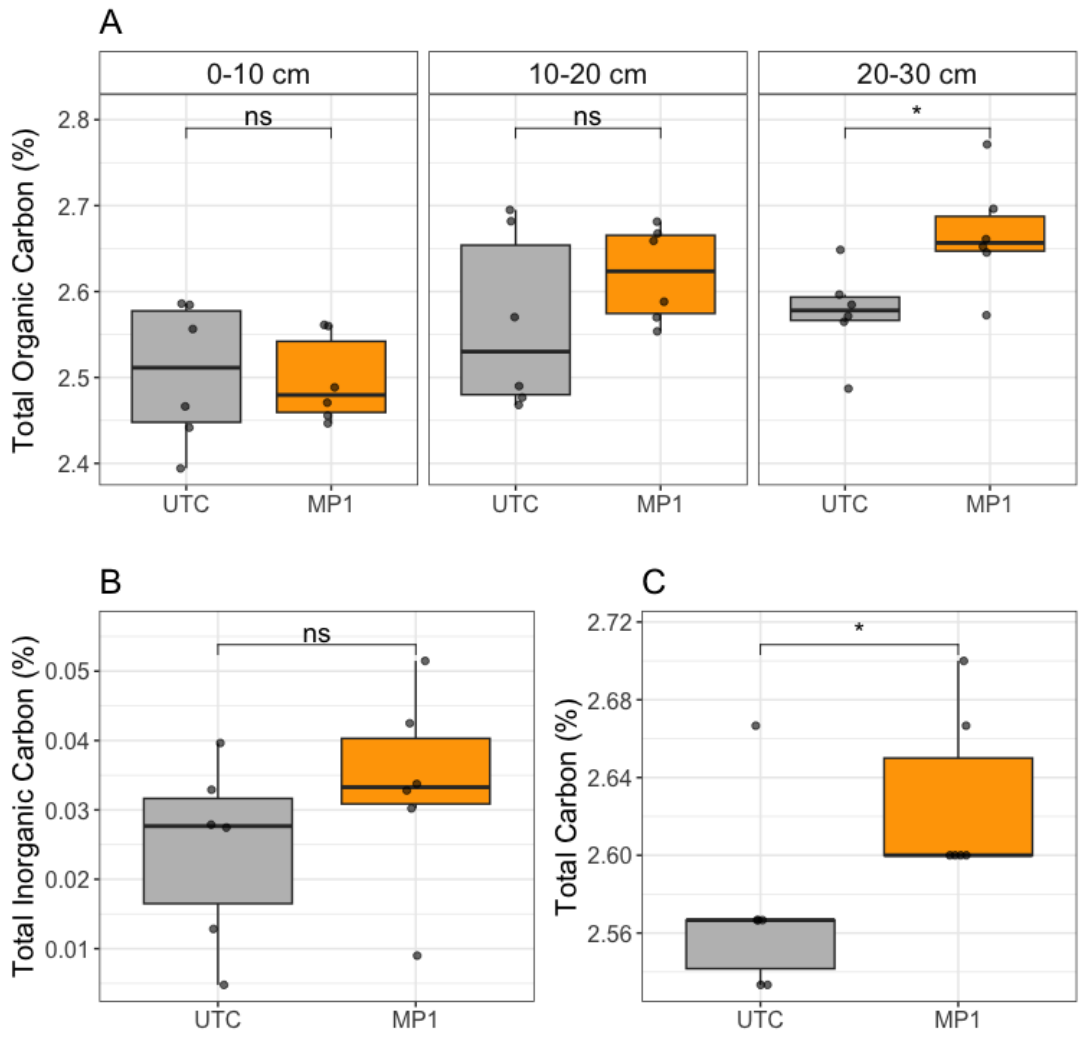

Figure 3. Total organic carbon **(A)**, total inorganic carbon **(B)** and total carbon **(C)** in MP1-treated and untreated control (UTC) columns. Wilcoxon signed-rank test, * $p < 0.05$, ns: not significant, $N = 6$. Note that y-axes are scaled to the data range to clearly visualize the distribution and variability across treatments.

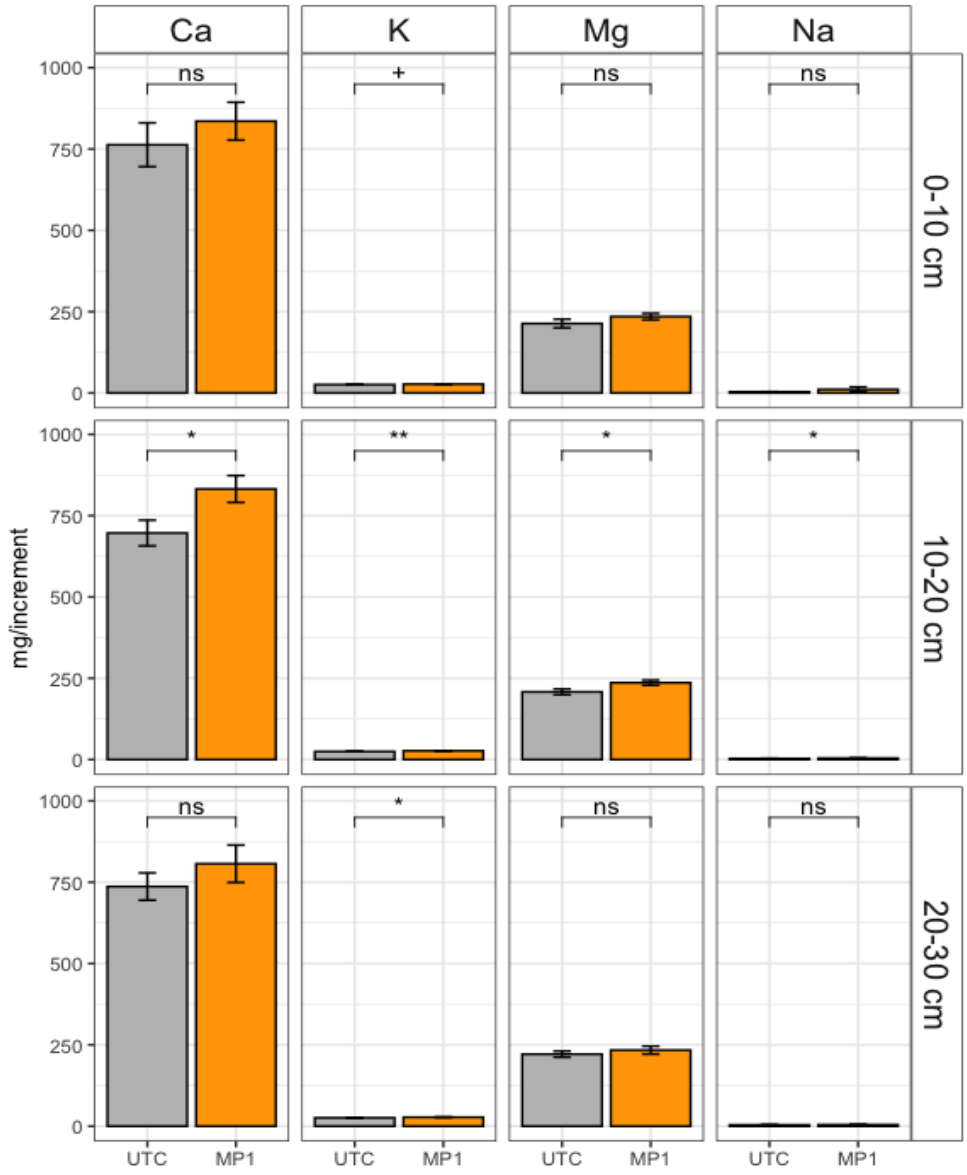

Figure 4. Concentration per depth increment of base cations in the carbonate pool in MP1-treated and untreated control (UTC) columns. Student's t-test, * $p < 0.05$, ns: not significant, $N = 6$.

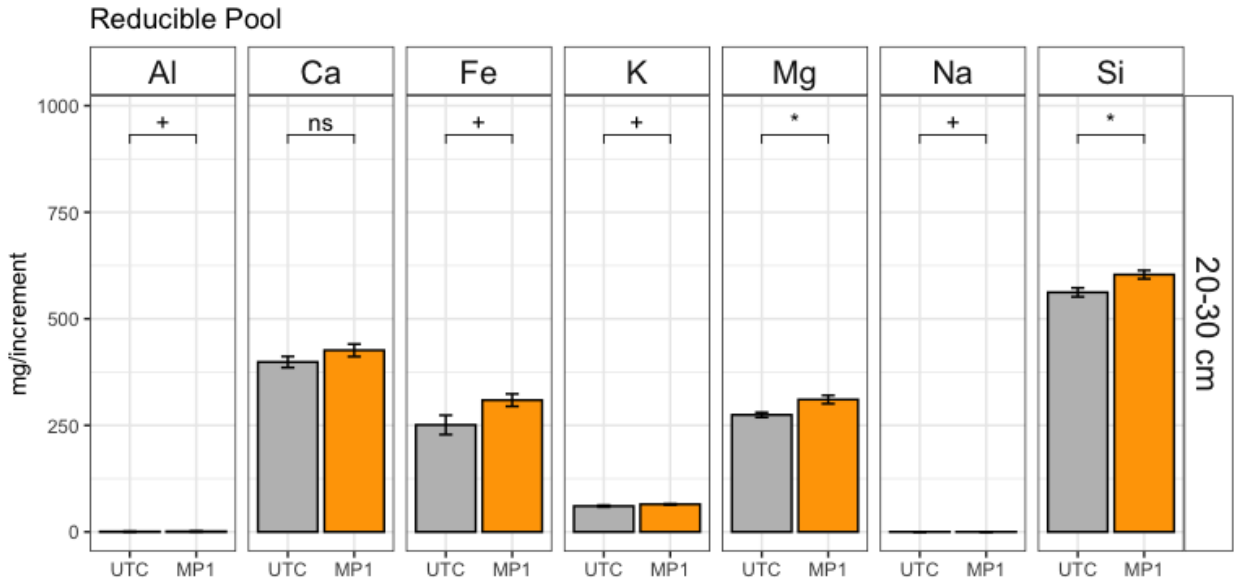

833

834 **Figure 5.** Concentration at the bottom depth of base cations in the reducible pool in MP1-treated

835 and untreated control (UTC) columns. Student's t-test, * $p < 0.05$, ns: not significant, $N = 6$.

836

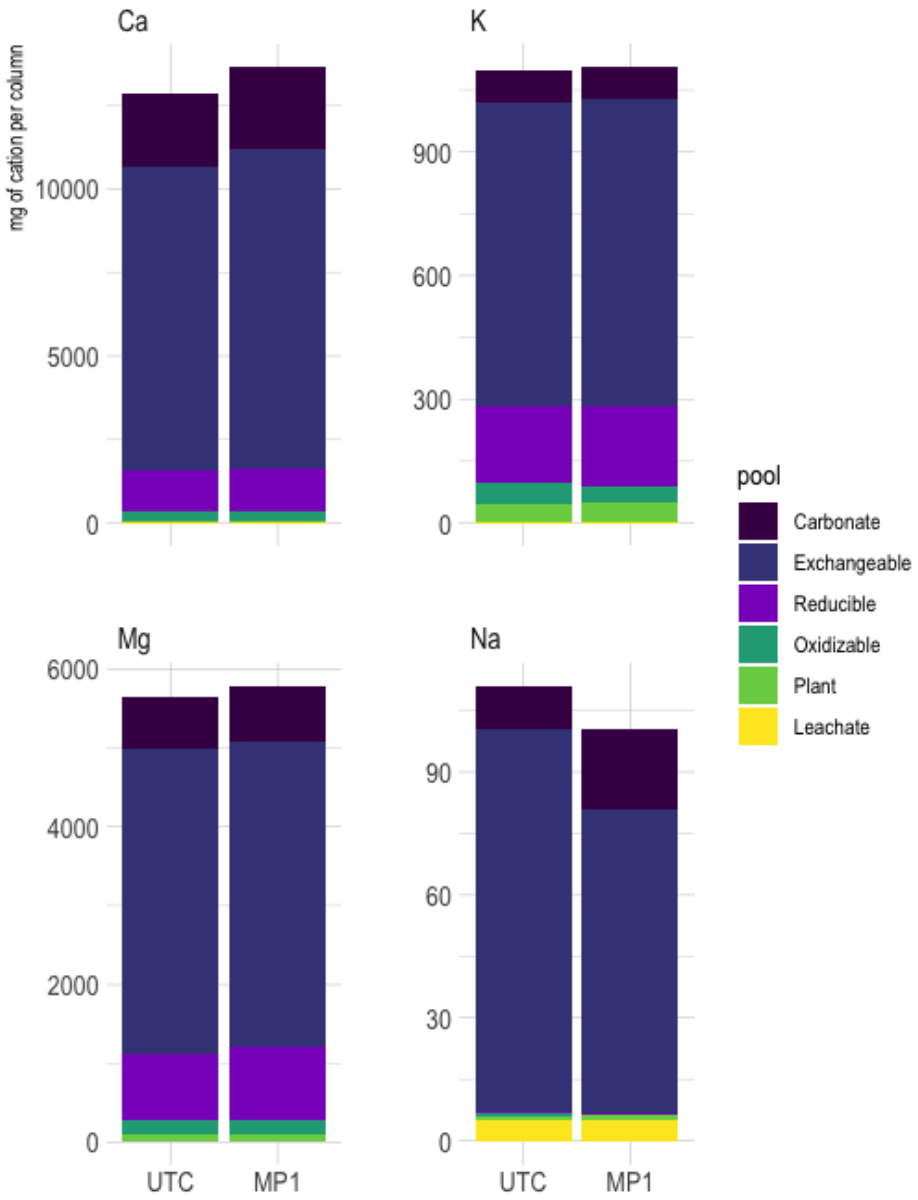

Figure 6. Cation mass-balance. Total mass of cations (in mg) per column, and their distribution between measured pools at the end of the 63-day experimental period. The carbonate, exchangeable, reducible, and oxidizable fractions are based on selective sequential extraction measurements.

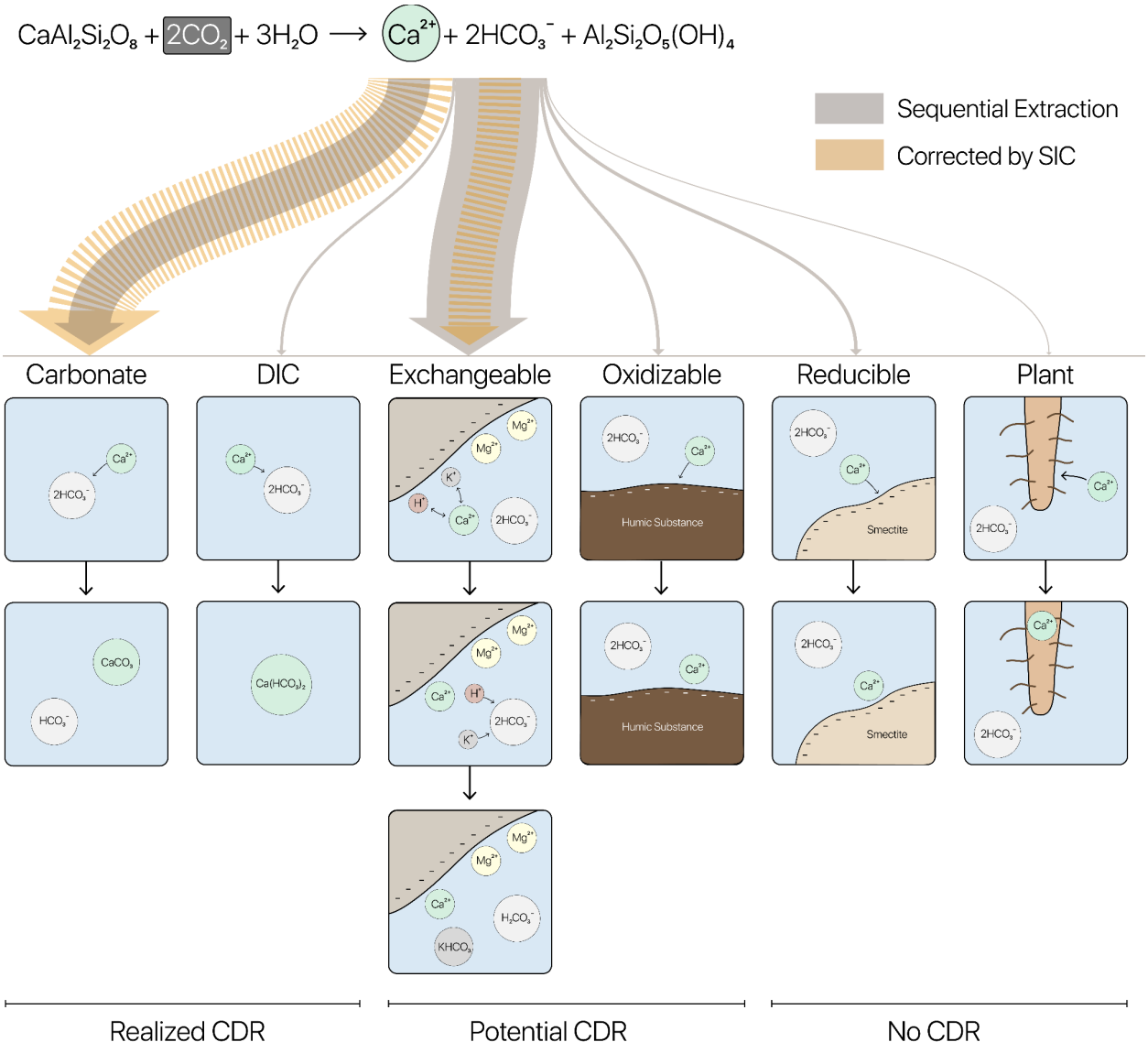

Figure 7. The mass balance approach reported here allows for tracking the fate of the observed increases in base cations from the acceleration of silicate weathering by the *B. subtilis* strain MP1. For simplification, we assume the observed increase in Ca ions is derived from the dissolution of anorthite mineral, and that the resulting Ca ions end up in one of six possible soil fractions: Carbonate, DIC, Exchangeable, Oxidizable, Reducible and Plant. The width of the gray arrows is proportional to the amount of new Ca ions that end up in one of the six characterized soil fractions. The width of the yellow arrows is proportional to the amount of new Ca ions that end up in the exchangeable and carbonate pools, corrected by the soil inorganic carbon measurement. Only Ca

851 ions that end up in the carbonate pool or are exported as dissolved inorganic carbon constitute
852 realized CDR. The exchangeable and oxidizable pools constitute potential future CDR, while the
853 reducible and plant pools represent cation scavenging that do not lead to CDR (no CDR).

Supplementary Information for "From silicates to soil carbonates: Tracing the cation budget of microbially-accelerated weathering"

Corey R. Lawrence[1], Harun Niron[2], Tania Timmermann[1], Philip D. Weyman[1], Yun-Ya Yang[1], Daniel Dores[1], Gonzalo A. Fuenzalida-Meriz[1,]*

[1] Andes Ag, Inc., Alameda, California, USA

[2] Biobased Sustainability Engineering (SUSTAIN), Department of Bioscience Engineering, University of Antwerp, Antwerp, Belgium

[*] Corresponding Author: Gonzalo A. Fuenzalida-Meriz, gonzalofuenzalida@gmail.com

FIGURES

878

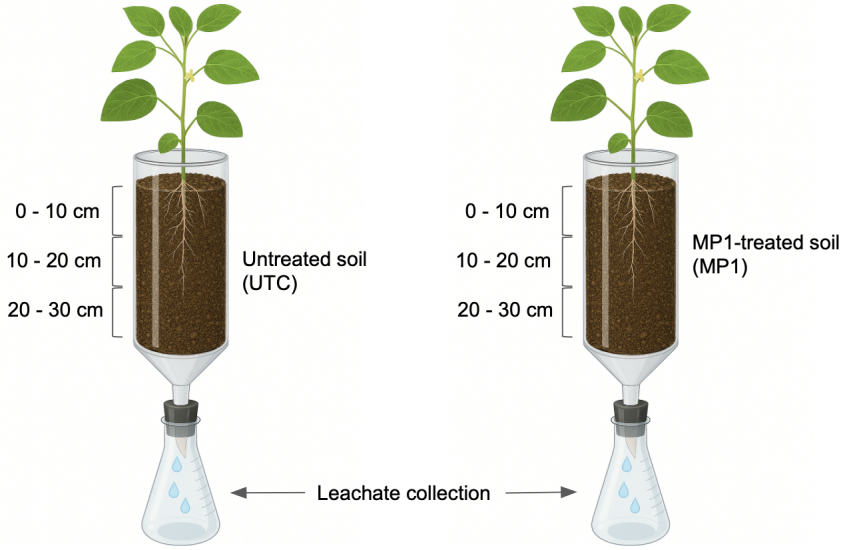

Treatment	MP1
UTC (x 6 columns)	-
MP1 (x 6 columns)	+

879

880 **Figure S1.** Scheme of the soil mesocosm study design.

881

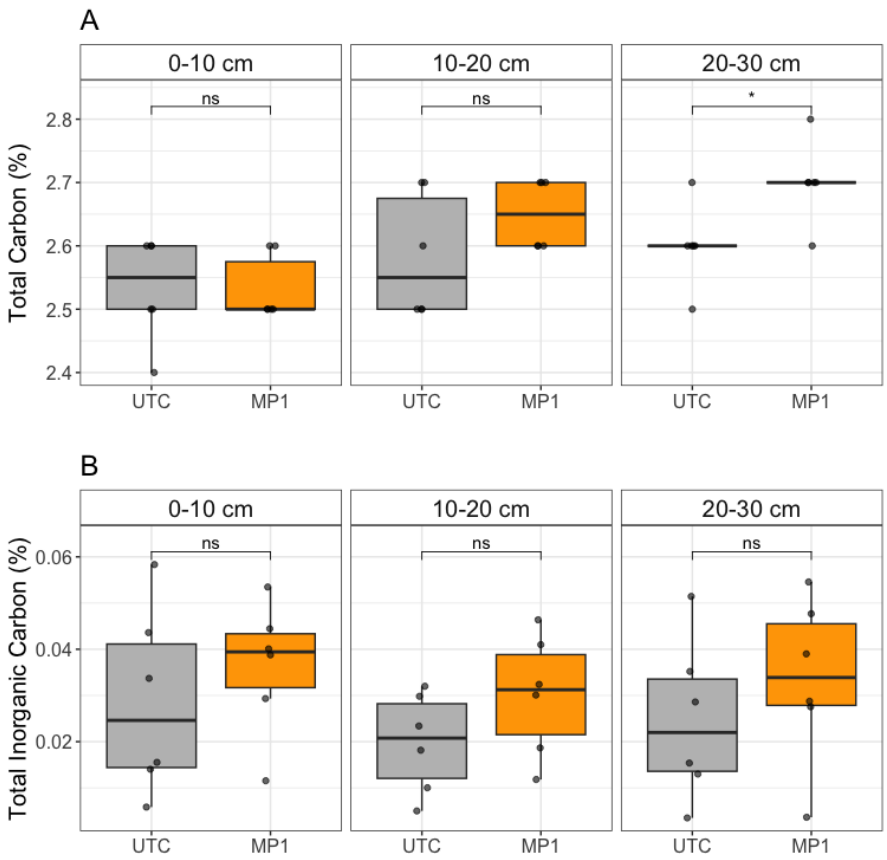

882

883 **Figure S2.** Total carbon **(A)** and total inorganic carbon **(B)** concentration per depth increment.

884 Student's t-test, * $p < 0.05$, ns: not significant, $N = 6$. Note that y-axes are scaled to the data range

885 to clearly visualize the distribution and variability across treatments.

886

887

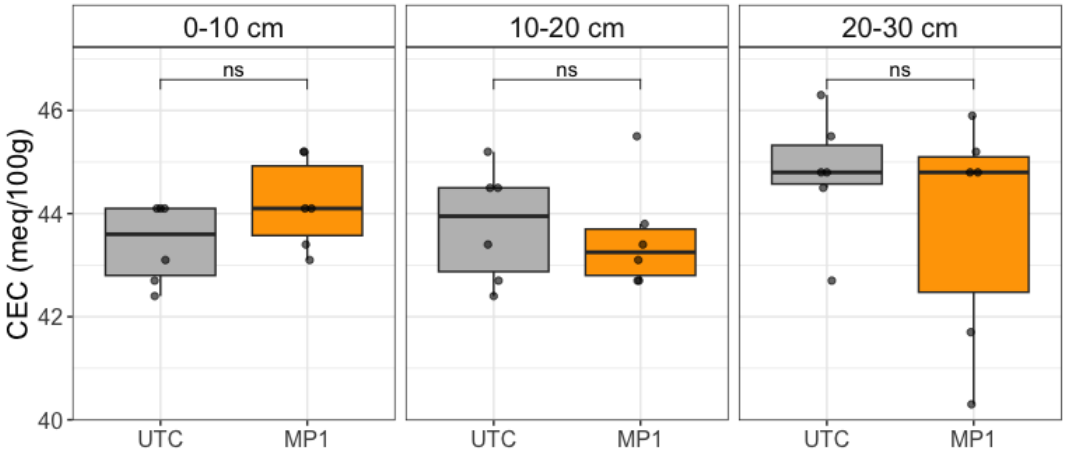

888

889 **Figure S3.** Soil Cation Exchange Capacity (CEC) per depth increment. Note that y-axes are

890 scaled to the data range to clearly visualize the distribution and variability across treatments.

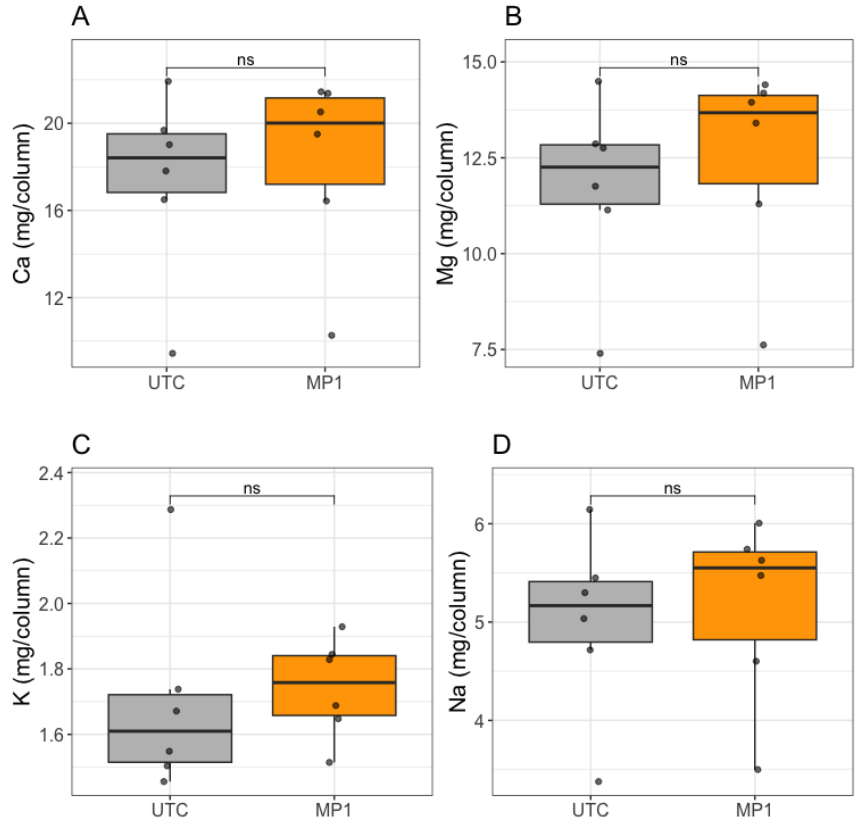

891

892 **Figure S4.** Base cations fluxes recovered from the leachate: Calcium **(A)**, magnesium **(B)**,

potassium **(C)** and sodium **(D)**. Note that y-axes are scaled to the data range to clearly visualize the distribution and variability across treatments.

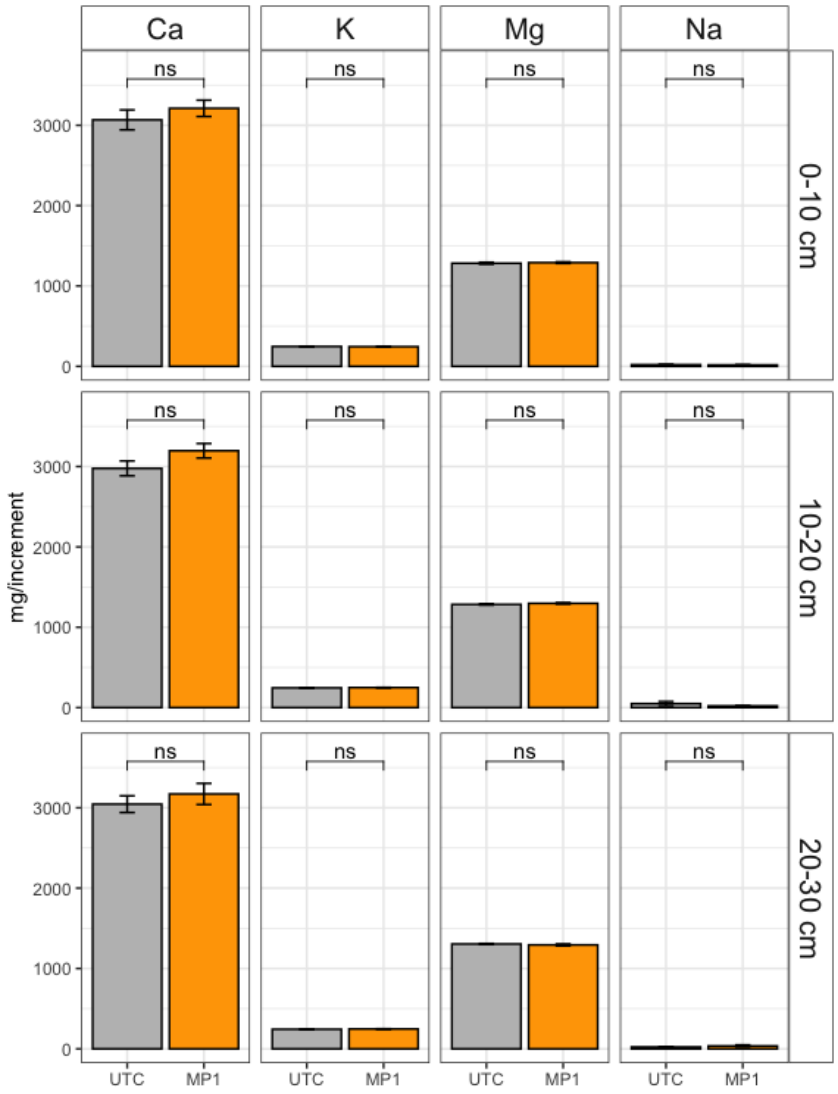

Figure S5. Concentration per depth increment of base cations in the exchangeable pool in MP1-treated and untreated control (UTC) columns.

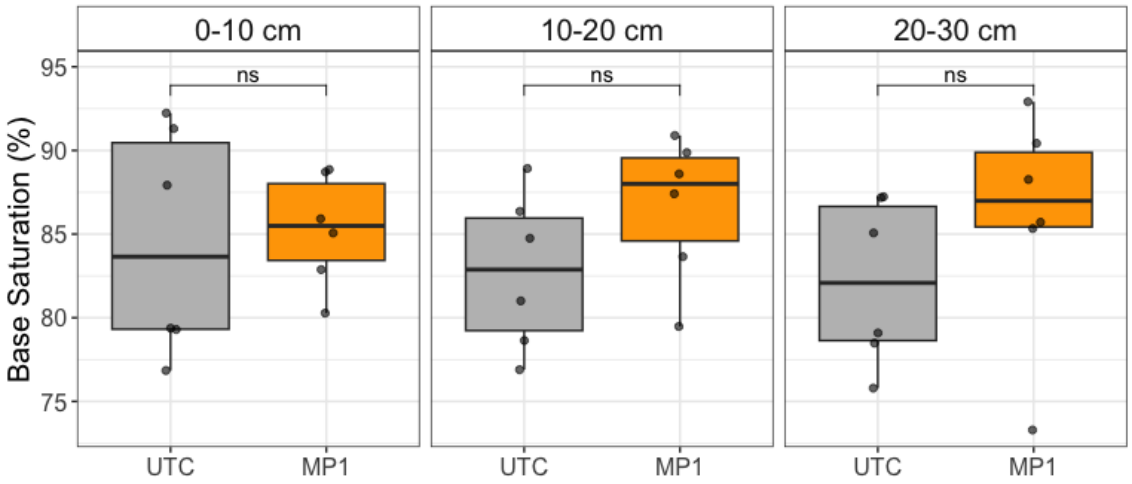

900

901 **Figure S6.** Base Saturation per depth increment. Calculated as ratio of exchangeable base

902 cations to total cation exchange capacity (both in units of mEq/100 g soil). Note that y-axes are

903 scaled to the data range to clearly visualize the distribution and variability across treatments.

904

905

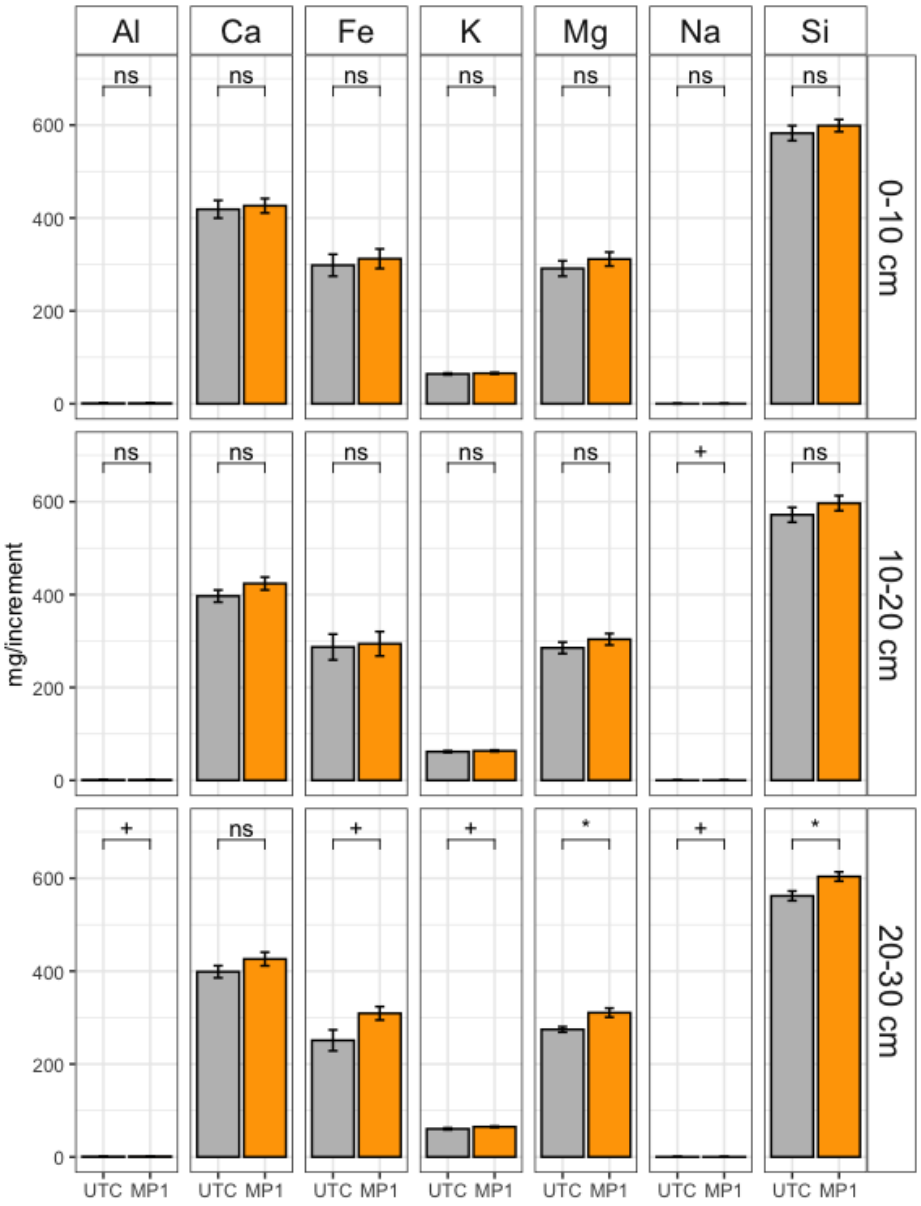

Figure S7. Concentration per depth increment of base cations in the reducible pool in MP1-treated and untreated control (UTC) columns. Student's t-test, * $p < 0.05$, + $p < 0.1$, ns: not significant, $N = 6$.

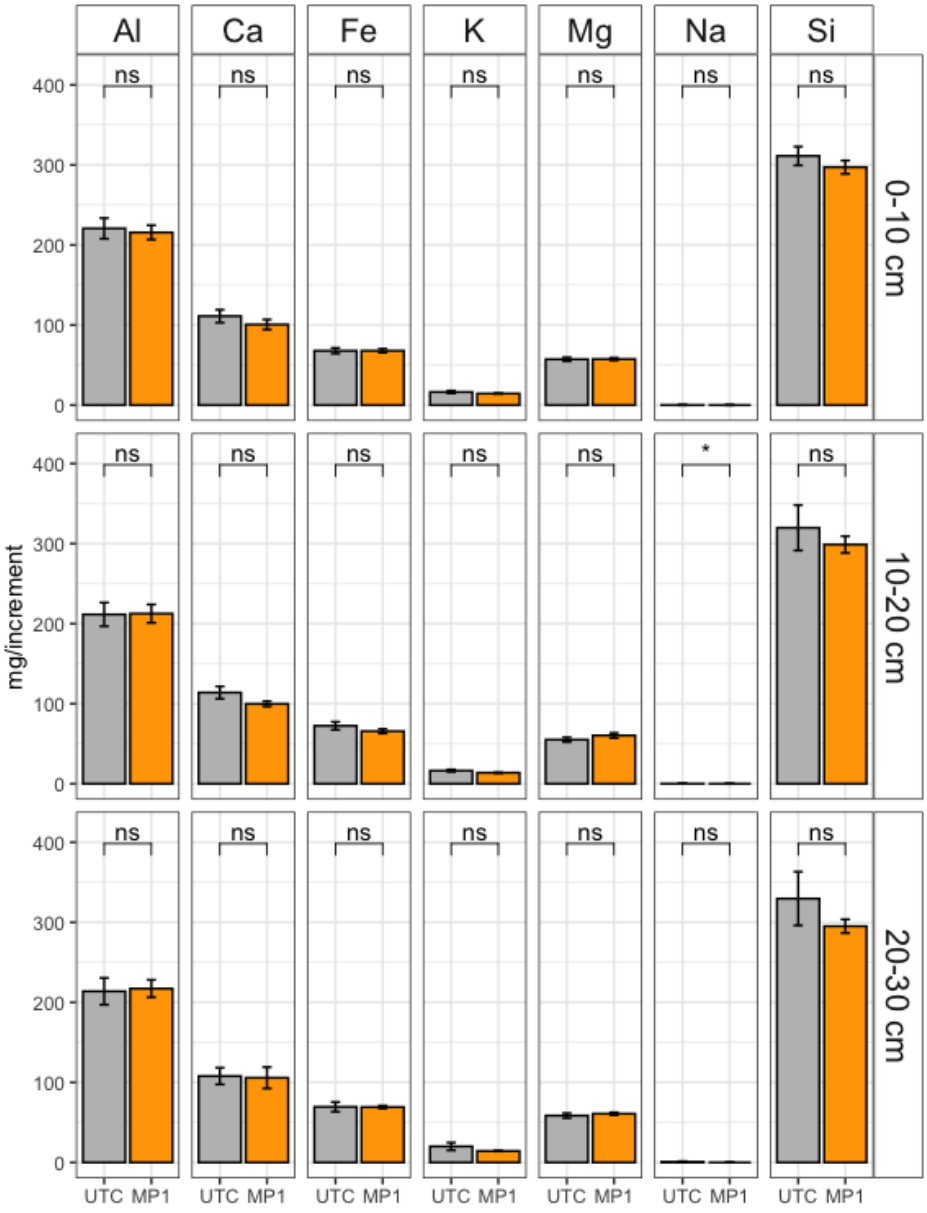

911

912 **Figure S8.** Concentration per depth increment of base cations in the oxidizable pool in MP1-

913 treated and untreated control (UTC) columns. Student's t-test, * $p < 0.05$, ns: not significant, $N =$

914 6.

915

916

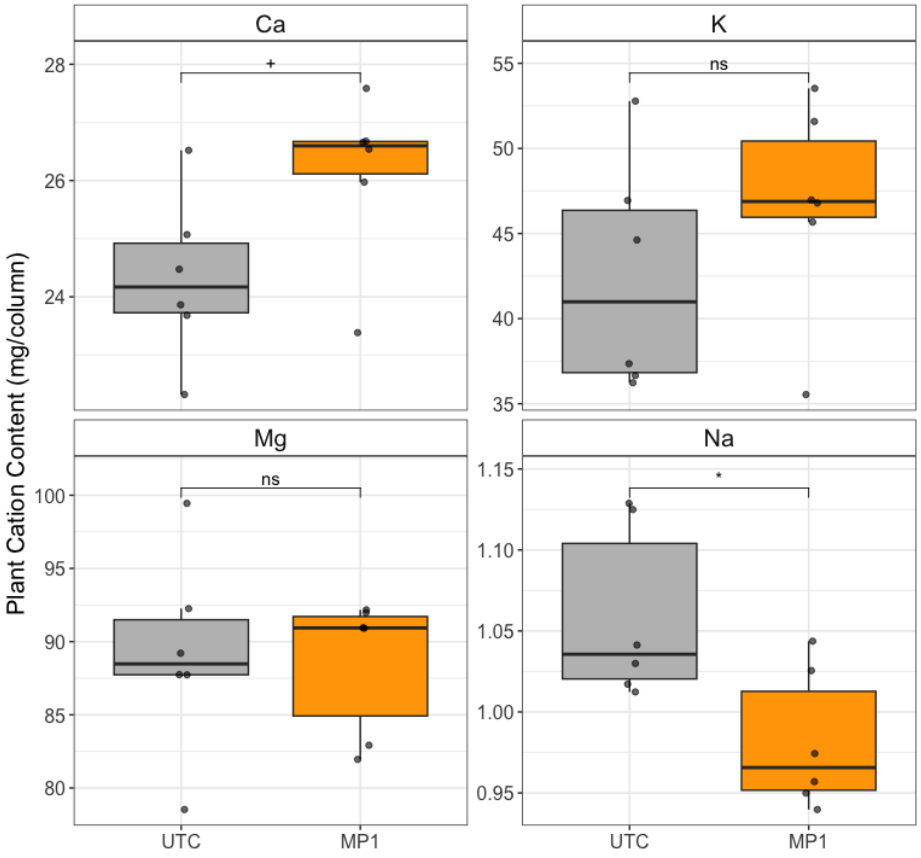

Figure S9. Plant pool cation content per column. Student's t-test, * $p < 0.05$, + $p < 0.1$, ns: not significant, $N = 6$.

928 **TABLES**

929

930 **Table S1.** Quantitative mineralogy for the SBX70 soil. Estimates of mineral classification and
931 corresponding abundances are based on SEM-EDS data. Note that the total feldspar abundance
932 represents the sum of individual feldspar types (italicized).

Mineral Type	Abundance (%)
Quartz	65
Total Feldspars	28
Albite	*10*
Oligoclase/Andesine	*9*
Orthoclase	*8*
Other Feldspars	*1*
Phyllosilicates	5
Other/Unidentified	2

933

934

935 **Table S2.** Abundance of major oxides measured by XRF in the SBX70 soil. Loss-on-ignition
936 (LOI) represents the mass of volatile compounds in the sample, including organic matter and
937 structural water in clays.

Elemental Oxide	Soil (wt %)
SiO_2	62.5
TiO_2	0.6
Al_2O_3	11.7
FeO	3.8
MnO	0.1
MgO	1.6
CaO	1.3
Na_2O	1.0
K_2O	2.0
P_2O_5	0.1
LOI	*15.0*

938

939

940 **Table S3.** Concentration and percentages of cations present in each pool at the end of the 63-day

941 experimental period. The concentrations represent the mean of 6 columns and ± its standard error.

	Ca		Mg		K		Na	
POOL (mg/column)	**UTC**	**MP1**	**UTC**	**MP1**	**UTC**	**MP1**	**UTC**	**MP1**
Carbonate	2196 ± 129 (17.1%)	2474 ± 142 (18.1%)	643 ± 28 (11.4%)	705 ± 28 (12.2%)	76 ± 1 (6.9%)	81 ± 1 (7.4%)	11 ± 1 (9.6%)	20 ± 8 (19.6%)
Exchangeable	9089 ± 289 (70.6%)	9579 ± 303 (70.0%)	3872 ± 289 (68.7%)	3881 ± 303 (67.0%)	736 ± 4 (67.2%)	741 ± 3 (66.9%)	93 ± 28 (83.8%)	74 ± 13 (74.0%)
Reducible	1214 ± 41 (9.4%)	1276 ± 40 (9.3%)	851 ± 30 (15.1%)	926 ± 26 (16.0%)	187 ± 5 (17.0%)	194 ± 3 (17.5%)	<1 (0.4%)	<1 (0.4%)
Oxidizable	333 ± 21 (2.6%)	306 ± 11 (2.2%)	171 ± 5 (3.0%)	179 ± 4 (3.1%)	53 ± 6 (4.8%)	42 ± 1 (3.8%)	1 (0.8%)	0 (0.0%)
Plant	24 ± 1 (0.2%)	26 ± 1 (0.2%)	89 ± 3 (1.6%)	88 ± 2 (1.5%)	42 ± 3 (3.9%)	47 ± 3 (4.2%)	1 (1.0%)	1 (1.0%)
Leachate	17 ± 2 (0.1%)	18 ± 2 (0.1%)	12 ± 1 (0.2%)	12 ± 1 (0.2%)	2 (0.2%)	2 (0.2%)	5 (4.5%)	5 (5.1%)
TOTAL (mg/col)	**12874 ± 320**	**13680 ± 338**	**5638±46**	**5792 ± 45**	**1096 ± 9**	**1108 ± 5**	**111 ± 28**	**101 ± 15**
Δ (mg/col)		**+806**		**+154**		**+12**		**-10**
TOTAL (mEq/col)	**642.4**	**682.6**	**463.9**	**476.5**	**28.0**	**28.3**	**4.8**	**4.4**
Δ (mEq/col)		**+40.2**		**+12.6**		**+0.3**		**-0.4**

942

943